Ferroelectric domain walls for nanotechnology

Dennis Meier and Sverre M. Selbach

Department of Materials Science and Engineering, NTNU Norwegian University of Science and Technology (NTNU), 7043 Trondheim, Norway

dennis.meier@ntnu.no, selbach@ntnu.no

Abstract | Ferroelectric domain walls have emerged as a new type of interface, where the dynamic characteristics of ferroelectricity introduce the element of spatial mobility, allowing for real-time adjustment of position, density and orientation of the walls. Because of electronic confinement, their distinct symmetry and chemical environment, the spatially mobile domain walls offer a wide range of functional electric and magnetic properties, representing excellent 2D components for the development of more agile next-generation nanotechnology. In this Review, we discuss how the field of domain wall nanoelectronics evolved from classical device ideas to advanced concepts for multilevel-resistance control in memristive and synaptic devices. Recent advances in modelling and atomic-scale characterization provide insight into the interaction of ferroelectric domain walls and point defects, offering additional routes for local property design. We also explore the discovery of functional domain walls in improper ferroelectrics and the intriguing possibility to develop the walls themselves into ultra-small electronic components, controlling electronic signals via their intrinsic physical properties. We conclude with a discussion of open experimental challenges and emergent domain wall phenomena that may play an important role for the future directions of the research.

Interfaces in oxide materials are a rich source for emergent phenomena and offer exciting opportunities for fundamental and applied research.[1,2] The prospect of interface-enabled physical properties can be traced back to symmetry considerations formulated already during the 19th century by Neumann and Voigt. They realized that the symmetry of a physical property is at least as high as the symmetry of the host material, generalizing the symmetry-property relation of crystals. Because of this universal relation, novel physical phenomena can be expected to arise when symmetry is broken. Symmetry breaking can occur spontaneously at a phase transition, but it can also be engineered to create new physical properties on demand. A classic example of interface-enabled functionality is p- and n-type semiconductors. Individually, such semiconductors have very limited technological potential, but once brought in contact, inversion symmetry is broken and a pn-junction with nonreciprocal direct current (d.c.) response is formed. This is the defining property of a diode, representing the most basic type of semiconductor device and one of the most crucial electronic building blocks in today`s technology. Herbert Kroemer's famous phrase "the interface is the device" referred to such traditional semiconductors,[3] but it has now become clear that the statement is equally true for oxide electronics.[4] In fact, interface-enabled functionality pervades all modern application-oriented sciences and technologies. For example, in the fields of spintronics[5] and skyrmionics[6], interface phenomena are utilized to engineer magnetic exchange interactions and produce functional non-trivial topological spin textures.[7,8] Furthermore, oxide interfaces are employed to control electronic transport,[9] as well as introducing epitaxial strain as a new control knob for tuning existing and inducing new properties.[10]

Domain walls in ferroelectric oxides are attracting attention as a completely new type of functional interface,[11] expanding the seminal research on domain walls in ferroelastic materials towards systems that exhibit a spontaneous electric polarization.[12,13] The domain walls naturally occur in ferroelectric materials where they separate the domains, that is, chemically identical regions that differ only in the orientation of the electric polarization.[14] Because of this, domain walls are sometimes referred to as homo-interfaces to distinguish them from conventional (hetero-)interfaces, such as the aforementioned pn-junction or interfaces in thin film multilayers. However, just like the artificially created oxide interfaces, domain walls display reduced dimensionality and different symmetry than the host material, giving rise to physical properties not found in the surrounding domains.[11,15] It has been demonstrated, for instance, that domain walls can display polarity[16] or magnetic order[17] even if forbidden in the bulk.[18] Furthermore, they can exhibit enhanced or reduced electronic conductivity and – in contrast with traditional hetero-interfaces – are spatially mobile which has already been reviewed in detail in REFS.[18–23]. In response to applied electric fields, ferroelectric domains can appear, change size or vanish, which implies that domain walls can be created, moved, and erased on demand. This ability allows for real-time adjustment of the domain wall position, density and orientation, which greatly extends the flexibility regarding the utilization of oxide interfaces and enables the design of future, more agile, domain-wall-based nanotechnology.[24]

In this Review, we discuss the evolution and the state of the art of the field of domain wall nanoelectronics. A specific focus will be on the rapid development of related device concepts and the transformative change that is taking place: Instead of serving as active components in a much larger device architecture, the domain walls themselves are now turning into devices. The transition from "walls serving in devices" to "walls acting as devices" becomes possible by utilizing their intrinsic physical properties and emergent electronic correlation phenomena. This approach is appealing as it breaks the mould of classical device architectures and fully capitalizes on the quasi-2D nature of the domain walls, facilitating ultra-small feature size and conceptually new

opportunities for the design of electronic building blocks and circuitry at the nanoscale. For readers who are looking for an introduction to the fundamentals, a more extensive discussion of the physical properties at ferroelectric domain walls and the early device concepts, we refer to previous reviews covering these particular aspects.[11,18–24]

We begin with a short overview of the original concepts for applications of ferroelectric domain walls. The direct observation of conducting ferroelectric domain walls in an otherwise insulating material[25] sparked an intensive search for new ways and materials to implement domain-wall-based electronics. We then discuss how the progress in experiment and theory propelled our understanding of the microscopic structure of domain walls and their interaction with point defects. This knowledge provides new grounds for the creation of unusual electronic states of matter and local chemical composition, giving rise to advanced domain wall functionality beyond just conductance. We continue discussing functional properties that have been discovered due to the inclusion of more exotic, non-conventional systems, where the ferroelectric polarization arises as a secondary effect driven by, for example, a lattice distortion or magnetic order (improper ferroelectrics [BOX 1]).[26,27] The important difference compared to conventional, proper ferroelectrics is that the primary order parameter is not the electric polarization, which promotes the natural formation of a plethora of different types of functional domain walls. We then have a closer look at property engineering at improper ferroelectric domain walls and how these can be used to emulate the behavior of electronic components. For nanotechnology, the possibility to utilize intrinsic properties of stationary domain walls to control electrical signals, rather than writing and erasing them, offers completely new prospects for the design of devices and circuitry. Finally, we address open challenges and future perspectives concerning application opportunities for domain walls in ferroelectrics and we discuss different directions this field may evolve in.

Classical domain wall nanoelectronics

Controlling resistivity by writing and erasing domain walls. Already in 1973, enhanced electrical conductivity at ferroelectric domain walls and possibilities for device applications were discussed.[28] Although their local conductivity was not accessible at that time, it was argued that domain walls where the polarization P of the adjacent domains meets in tail-to-tail or head-to-head configuration [BOX 1] can be utilized to control electrical currents. For these polarization configurations substantial bound charges arise at the domain walls, leading to locally diverging electrostatic potentials that require screening. One way of screening this electrostatic potential is to redistribute free electrons and holes, which can lead to considerable charge carrier densities at the domain walls. For example, an electron density of ~10^{14} per cm^2 is required to screen head-to-head walls in $BaTiO_3$ (proper ferroelectric, $P \approx 26$ μC/cm^2)[29–31]. Because of the accumulation of free carriers, the domain wall conductivity can be expected to be much higher than in the surrounding bulk.[32,33] In the original device concept, it was suggested to utilize this phenomenon and control resistivity via charged ferroelectric domain walls (Fig. 1a).[28]

In 2009, conductive atomic force microscopy (cAFM) was applied to directly measure the conductance at different types of ferroelectric domain walls in $BiFeO_3$. The resistivity was estimated to be as low as 1-10 Ωm, which is five to six orders of magnitude lower than in the bulk.[25] The work on $BiFeO_3$ went beyond previous scanning electron microscopy (SEM) studies on $BaTiO_3$ [34] and $LiNbO_3$ [35] which indicated unusual electronic responses at ferroelectric domain walls, and provided first direct and quantifiable evidence for their enhanced electronic conduction. Furthermore, the general feasibility of domain-wall based electronics was demonstrated, realizing

132 multi-level resistance control via the injection and deletion of conducting domain walls (Fig. 1b).
133 These experiments established ferroelectric domain walls as functional nanoscale entities that can
134 play an active role in electronic devices, serving as re-configurable, ultra-small conducting
135 channels.

136 This discovery triggered world-wide attention and a rapid expansion of the field, which led to the
137 observation of conducting ferroelectric domain walls in multiple materials, including proper
138 ($BaTiO_3$,[30,31] $LiNbO_3$,[36,37] $BiFeO_3$,[25,38–43] $PbZr_{1-x}Ti_xO_3$ (PZT),[44–47] $KTiOPO_4$[48]) and improper (RMnO$_3$ (R
139 = Sc, Y, In, Dy to Lu),[49–54] $Cu_3B_7O_{13}Cl$,[55] $(Ca,Sr)_3Ti_2O_7$[56]) ferroelectrics. Besides novel application
140 opportunities, the fundamental mechanisms that can give rise to enhanced conduction at domain
141 walls were investigated. Three main mechanisms have been identified, which can be classified as
142 intrinsic or extrinsic effects as discussed, for example, in REF.[18]. Intrinsic effects include (i) a
143 reduction in the electronic band gap due to a subtly different electronic structure at domain walls,
144 and (ii) a shift of the valence and conduction bands caused by domain wall bound charges. Domain
145 wall conduction enhanced by such intrinsic effects is desirable whenever resistivity is controlled
146 via the injection and deletion of domain walls to facilitate fast response times and avoid
147 degradation, e.g., from pinning of domain walls by point defects. In contrast, extrinsic domain wall
148 conduction relies on point defects [BOX 2], being driven by (iii) the segregation of charged point
149 defects towards or away from the domain walls along with concomitant charge compensating
150 electrons or holes. It is important to note, however, that in real materials all these mechanism (i)-
151 (iii) may be at play and their deconvolution can be very challenging. In addition, comprehensive
152 information about the electronic bulk properties, including carrier densities and mobilities, is
153 often missing which complicates the evaluation of domain-wall specific responses. This is because
154 of large resistivities and the sensitivity of oxide materials to high electric voltages, which can make
155 quantitative transport measurements highly non-trivial. In fact, in several studies, the type of
156 majority carriers in the bulk (electrons or holes) has been inferred from cAFM
157 measurements.[50,55,56] As cAFM is a two-point measurement, however, multiple conductance
158 contribution are simultaneously measured as recently analyzed in detail for domain walls in
159 $Er_{0.99}Zr_{0.01}MnO_3$.[57] Thus, in order to achieve a better understanding of the domain wall conduction
160 at the quantitative level, correlated investigations of the electronic bulk properties are desirable.

161 ***Domain-wall memory cells and memristive devices*****.** Following the proof-of-concept work on
162 $BiFeO_3$,[25] the majority of research initially focused on the creation and manipulation of individual
163 domain walls with intrinsically enhanced conduction to control electronic signals and store
164 information. In 2014, for example, the idea of an electronic device[58] where charged domain walls
165 are the essential building block was patented, incorporating the discovery of a 2D electron gas at
166 head-to-head domain walls in $BaTiO_3$.[31] A first experimental breakthrough was the realization of
167 a model memory cell, where a single ferroelectric 71° domain wall was written and erased
168 between platinum electrodes deposited on the surface of a $BiFeO_3$ thin film to define non-volatile
169 ON (high current) and OFF (low current) states.[59] The concept was later refined to achieve a tri-
170 state domain-wall switch by controlling the charge state of the injected domain wall as illustrated
171 in Fig. 1c.[60] Unfortunately, the electrical currents passing through single $BiFeO_3$ domain walls are
172 still too low for typical device applications. Higher electrical conduction and an almost continuous
173 set of resistive states – varying by nearly 12 orders of magnitude – were measured on a 500 nm
174 thick $LiNbO_3$ single crystal when changing the density of conducting head-to-head domain walls.[61]
175 The emergence of conducting head-to-head walls in $LiNbO_3$ is known for a long-time[36] and record-
176 high current values have been reported.[37] However, the observation of the concerted response of
177 conducting head-to-head walls is intriguing as it facilitates the design of a new type of memristor,
178 expanding the field of domain-wall nanoelectronics into the realm of artificial synapses and

neuromorphic computing, complementing previous studies that utilized ferroelectric domains rather than domain walls (see, e.g., REF. [62] for a general review on neuromorphic computing).[63,64] Studies at the local scale indicate that a continuous set of resistive states may even be realized working with individual head-to-head domain walls in $LiNbO_3$, using sub-coercive voltage pulses to manipulate the domain wall orientation and, hence, its conductivity in a continuous way.[65,66] Furthermore, it was demonstrated that nonvolatile field-effect transistors can be realized using ferroelectric domain walls in $LiNbO_3$, functioning based on the reorientation of conducting head-to-head walls.[67]

Transient and dynamical domain wall responses. Another approach towards enhanced performance is to utilize energetically highly unfavorable domain wall configurations that occur only due to specific boundary conditions or transiently while external electric fields are applied. The switching of nanodomains in PZT, for example, was shown to yield strongly curved domain walls with fully charged 180° head-to-head sections, offering an up to three orders of magnitude higher carrier density than the bulk.[46] By creating such nanodomains, a local insulator-metal transition was driven and used to write multiple non-volatile resistive states in a single metal-ferroelectric contact. It was shown later that even 90° domain walls in PZT can develop metallic conductivity when they are forced to locally bend away from their ideal charge-neutral structure.[47] Following a similar approach, domain-wall enabled giant resistive switching in a 20 nm thick $BiFeO_3$ film was realized.[68] Here, repeated creation and annihilation of charged 71° domain wall segments within the film (length $\approx$10 nm) allowed to reversibly switch between two well-defined states with high and low resistivity and an on/off ratio of up to 10^5. Instead of using the domain walls themselves to encode information, it was demonstrated how the conducting walls can be used to read out domain states in ferroelectric memory devices.[69] While electrical fields applied parallel to the polarization direction had no effect on the resistance of the studied $BiFeO_3$ film, a significant increase in conductance was observed for electrical fields applied in the opposite direction. Currents of up to 14 nA were measured, originating from partial switching and the creation of conducting 71° domain walls, which stabilize only transiently for as long as the read-voltage is applied (Fig. 1d). Only recently, this concept was expanded toward $LiNbO_3$ based devices on Si wafers, representing an important breakthrough regarding the development and integration of domain-wall based technology. [70]

Dynamical aspects have been investigated in order to gain additional insight into the electronic transport properties[71] and expand domain wall nanoelectronics into the realm of alternating-current (a.c.) technology. Microscopy experiments performed in the microwave regime on hexagonal manganites (RMnO$_3$)[72] and ferrites (RFeO$_3$)[73], PZT[74] and $BiFeO_3$[75] revealed significantly enhanced a.c. conductivity at nominally neutral domain walls. The anomalous a.c. microwave conductivity can be several orders of magnitude larger than the d.c. currents and was attributed to bound-charge oscillations and domain wall roughening. Although the research is still at an early stage, the results are intriguing as they suggest that ferroelectric domain walls can be used to design nanoscale inductors and transformers, and potentially play a role also for radio-frequency applications.

Challenges associated with the classic approach. Several important cornerstones are now in place so that the step from proof-of-concept studies to domain-wall enabled nanotechnology is within reach. Although the typical electrical currents measured at most domain walls are in the pico- to nanoampere range,[11] local transport measurements on $LiNbO_3$ demonstrated that values > 1 μA are achievable,[37] which is large enough for driving read-out circuits in high-speed applications: As discussed in REF. [69], a domain wall current of 0.1 μA is needed to achieve a read time of 10 ns

225 (Johnson-Nyquist limit[76,77]). Furthermore, it has been shown that domain wall currents in $BaTiO_3$
226 and $LiNbO_3$ can be 10^9 and 10^{13} time higher, respectively, than in the bulk.[31,37] For comparison,
227 established Metal Oxide Semiconductor Field Effect Transistors (MOSFETs) operate with an on/off
228 ratio of 10^{10}.[78] While the exact carrier mobility at the domain walls remains to be quantified,
229 estimates based on pioneering Hall effect measurements on $ErMnO_3$ revealed that mobilities of
230 hundreds of $cm^2\ V^{-1}\ s^{-1}$ can occur at room temperature,[79] which is remarkably high compared to
231 the sheet carrier mobilities reported for other oxide systems.[80–83]

232 Up to now, the majority of application concepts applies the original principle, that is, the injection,
233 manipulation, and deletion of conducting ferroelectric domain walls to control electric
234 conductivity.[19,22,24] A downside of these concepts is that near-perfect materials with a low
235 concentration of point defects are necessary to achieve large on-off ratios and high endurance. As
236 we will discuss in detail in the next section, point defects can strongly interact with ferroelectric
237 domain walls, altering their electrical properties and reducing their mobility by pinning. One
238 fundamental problem is that the requirement of a low point defect concentration is counteracted
239 by the need to screen the diverging electrostatic potential at charged domain walls in proper
240 ferroelectrics. Recent studies showed that this problem can be mitigated by utilising charged
241 domain wall sections that are created only transiently,[69] at low-temperature,[47] or in sub-surface
242 regions. This way, the effects from point defect segregation are suppressed, representing helpful
243 guidelines for the design strategy of future devices. However, while the concept of writing and
244 erasing domain walls clearly achieves a step beyond conventional interfaces by making use of the
245 wall mobility, it does not break the mould of classical device architectures (see Fig. 1c).
246 Furthermore, functional properties beyond just conductance that have the potential to give a new
247 dimension to the established device concepts for ferroelectric domain walls remain to be utilized.
248 Examples include the emergence of unusual magnetic order[17], magnetotransport,[84–86] and
249 mechanical responses[87] at the walls, as well as their impact on heat transport[88–91] and photovoltaic
250 phenomena.[92–96] To functionalize the versatile electronic properties even further and benefit from
251 the atomic-scale feature size of ferroelectric domain walls, researchers now begin to develop
252 conceptually different strategies, incorporating the distinct interactions of domain walls and point
253 defects, as well as new materials beyond the classical proper ferroelectric perovskites.

254

255 Defect-enabled domain wall functionality

256 ***Designing properties with point defects*.** Recent advances in growth techniques have enabled the
257 synthesis of ferroelectric oxides with unprecedented precision. Thin-film ferroelectrics can be
258 grown layer-by-layer, controlling key properties such as epitaxial strain, stoichiometry, defect
259 density, and domain configuration, with the possibility of in-situ property monitoring during
260 growth.[10,97,98] At the same time, we have seen a rapid evolution in characterization techniques,
261 allowing researchers to investigate ferroelectric domain walls in a much more systematic way and
262 across all relevant length scales.[11] The crystallographic[99] and electronic structure[100,101], as well as
263 the local stoichiometry at domain walls can now be resolved with pico-meter precision and
264 surface-analysis techniques provide access to the domain wall dynamics, local electrostatics and
265 electronic transport.[11]

266

267

268

269 This level of accuracy and the concerted application of complementary state-of-the-art imaging
270 techniques is crucial for moving beyond the utilization of only intrinsic conduction phenomena
271 and benefit from the additional degrees of freedom that arise from extrinsic contributions and the
272 interactions of domain walls with point defects in general. A key observation in this context was
273 the correlation between oxygen vacancies and superconductivity at ferroelastic twin walls in WO_{3-}
274 $_{x}$,[12,13] which have also been proposed as chemical turnstiles[102] with enhanced ionic transport
275 compared to bulk. Similar to ferroelastic domain walls, the importance of point defects for the
276 properties of ferroelectric domain walls has been known all along and was also discussed in
277 connection with the first direct observation of charged 180° head-to-head domain walls in PZT.
278 Consistent with previous theoretical studies,[103] it was proposed that the domain wall bound
279 charges are either compensated by a local reduction of the titanium valency from Ti^{4+} to Ti^{3+}
280 (intrinsic) and/or oxygen vacancies (extrinsic).[104] The accumulation of oxygen defects and their
281 impact on the local conductance was confirmed by subsequent transport studies: In contrast to
282 the charged head-to-head domain walls in PZT nanodomains with metallic conductance (possibly
283 intrinsic),[46] a certain threshold density of oxygen vacancies is required to achieve enhanced
284 conductance at extended nominally neutral walls in PZT thin films.[45] This correlation indicates that
285 point defects can be used to functionalize ferroelectric domain walls and fine-tune their transport
286 properties following the standard practice in silicon technologies. In contrast to a century of
287 research on doped semiconductors, however, very little is known about how point defects and
288 dopants influence the electronic properties at ferroelectric domain walls. As experimental studies
289 at the relevant length scales used to be virtually impossible, researchers in the past heavily relied
290 on the interpretation of indirect macroscopic measurements when it came to the complex
291 phenomena that emerge due to the interactions of domain walls with point defects [BOX 2].

292 ***First principles studies of domain wall–point defect interactions.*** First principles electronic
293 structure calculations had great success in filling the experimental gaps, establishing a link
294 between point defects and the domain wall structure, strain effects and electronic properties.
295 However, despite the breakthroughs in explaining the mechanisms of ferroelectricity in bulk
296 ferrolectrics[105–108], and calculations of the local crystallographic and electronic structure at
297 ferroelectric domain walls[25,50,109–119] (see, e.g., REF. [120] for a comprehensive review), a
298 corresponding understanding of domain wall–point defect interactions has evolved comparatively
299 slowly. An obvious reason is that while the crystal structure and electronic properties of, e.g., bulk
300 $PbTiO_3$ can be captured by a 5-atom cell, the construction of supercell models with both domain
301 walls and point defects[121] requires at least an order of magnitude more atoms.

302 Initially, the main goal was to determine to what extent point defects influence domain wall
303 dynamics, acting as pinning centers (Preisach model)[122] that contribute to effects such as pinched
304 hysteresis loops, hardening, and fatigue[123–125]. To evaluate the impact of point defects, the
305 segregation enthalpy was calculated as the energy difference for a point defect at a domain wall
306 compared to a point defect within the bulk. In $PbTiO_3$, for example, density functional theory (DFT)
307 calculations showed that oxygen vacancies at both 180° [109,126–129] and 90° [130] domain walls are
308 more stable than within the bulk and, hence, promote domain wall pinning. Similarly, the higher
309 energy barrier for migration of neutral 180° domain walls across oxygen vacancies calculated for
310 $BaTiO_3$[131] and $LiNbO_3$[132] reflects that domain walls within these ferroelectrics tend to get pinned
311 by vacancies. Going beyond oxygen defects, the impact of impurities and dopants on the domain
312 wall mobility was investigated, e.g., by considering platinum impurities in $PbTiO_3$[126] and zirconium
313 dopants in $YMnO_3$[133].

314 It has been commonly assumed that the static calculations of negative segregation enthalpy
315 between a defect/dopant and a domain wall also imply pinning and a higher domain wall
316 migration barrier. However, no such connection was found for calcium and titanium dopants in
317 $YMnO_3$.[133] Thus, it remains unknown whether moving and static domain walls experience the same
318 interaction with point defects. In general, the microscopic origins of, and differences between,
319 static binding energy and dynamic pinning of domain walls by point defects is largely uncharted
320 territory.

321 With the discovery of conducting domain walls in ferroelectrics and the advent of domain wall
322 nanoelectronics, the impact of point defects on the electronic density of states at domain walls
323 moved more into the focus of first-principles studies, exploring opportunities to control and fine-
324 tune the local transport behavior. In $BaTiO_3$, the interaction of oxygen vacancies with charged
325 domain walls was predicted to increase the n-type conductivity at head-to-head domain walls and
326 reduce the p-type conductivity at tail-to-tail domain walls.[134] Aside from perovskite systems, the
327 impact of oxygen vacancies on the electronic domain wall structure has been investigated in less
328 dense ferroelectrics with hexagonal crystal structure. In was found that, in contrast to $PbTiO_3$,
329 $BaTiO_3$, and $LiNbO_3$, oxygen vacancies do not have a propensity to accumulate at neutral 180° in
330 hexagonal manganites[135] and ferrites[136], thus not playing a decisive role for domain wall
331 conductivity. Oxygen interstitials, on the other hand, which are readily accommodated in the
332 hexagonal crystal structure[137], were shown to accumulate at neutral 180° domain walls in
333 $YMnO_3$[138,139], giving rise to enhanced electronic hopping conductivity. It is clear that oxygen
334 defects also co-determine the electronic structure at the charged head-to-head and tail-to-tail
335 domain walls in hexagonal manganites[140], but quantitative insight is missing and consequences
336 resulting from the mixed ionic-electronic nature of the conductance at defect-rich charged domain
337 walls remain unknown.

338 Recent advances in materials characterization have improved the situation and allow for
339 determining structural and electronic properties at domain walls much more accurately. Modern
340 scanning-transmission-electron microscopy techniques, for example, facilitate picometer-precise
341 measurements of atomic positions that can guide first-principles studies and help evaluating
342 calculated results. Because of this opportunity, it has become quite common in the field that
343 experiment and theory work hand in hand. This concerted application has significantly pushed the
344 fundamental understanding of the complex domain wall–point defect interactions and enabled
345 property control at the atomic scale as illustrated by the following examples.

346 ***Strain-engineered electronic domain wall response*.** Improved control of epitaxial strain in thin
347 films has led to the discovery of new functionalities also at domain walls. One example is the
348 recent study on $SrMnO_3$ films with strain-induced polar order (1.7 % tensile strain). The strained
349 $SrMnO_3$ films exhibit textured patterns of highly insulating domain walls which are oriented along
350 the crystallographic [100] and [010] directions (Fig. 2a).[141,142] The walls separate the material into
351 nano-regions that can be individually charged, acting as nano-capacitors. Here, the domain walls
352 owe their functionality to a strain-induced increase in the concentration of oxygen vacancies. For
353 the oxygen vacancies it is energetically favorable to accumulate at the domain walls, forming
354 columns that suppress electronic conduction. Vice versa, the controlled injection of oxygen
355 vacancies, and charged defects in general, may be used to pin domain walls and selectively change
356 their electronic conduction compared to unpinned walls that have a lower defect density.

357 Besides strain engineering in thin films, built-in gradients in strain and polarization at ferroelectric
358 domain walls can be exploited to attract or repel point defects and tune their electronic response.

359 In $BiFeO_3$, lattice-strain gradients across neutral 109° head-to-tail walls correlate with an
360 accumulation of bismuth vacancies, which are charge compensated by Fe^{4+} ions (Fig. 2b).[100,143] The
361 coexistence of Fe^{4+} and Fe^{3+} at the domain walls promotes p-type conductivity via electron-hole
362 hopping, i.e., a defect chemistry driven effect (extrinsic) that can add to – or even dominate – the
363 intrinsic properties that arise from a local reduction in the band gap or band bending caused by
364 domain wall bound charges. Different from the neutral 109° head-to-tail walls in $BiFeO_3$,
365 accumulation of oxygen vacancies was reported to play the key role for enhanced electronic
366 conduction at charged 109° walls in tail-to-tail configuration.[99,144] The accumulation is facilitated
367 by the tensile strain present at the walls, reflecting a strong correlation between local
368 deformations and defect accumulation, similar to the case of $SrMnO_3$ but with opposite
369 consequences for the local conductance.

370 The two examples of defect-enabled conductance at domain walls in $BiFeO_3$ reflect the impact of
371 point defects and their significance for the local transport behavior. By integrating defect
372 chemistry as control mechanism into device concepts, dynamic control of the domain wall
373 response becomes possible without the need to move or bend the walls. Instead, their behavior
374 can be adjusted, for example, by tuning the oxygen off-stoichiometry via annealing under oxidizing
375 (O_2), inert (N_2) or even reducing (e.g. 5% H_2) conditions.[145] Thermo-atmospheric control is
376 appealing as it is, in principle, completely reversible and can enable re-configurable domain wall-
377 based circuits. Additionally, it can expand domain wall nanoelectronics into the realm of sensor
378 technology, where changes in environmental conditions (e.g., temperature and oxygen partial
379 pressure) are resolved as changes in domain wall conductance. Such domain-wall-based sensors
380 could be operated either individually or in dense arrays to detect environmental changes with
381 nanoscale spatial resolution. Thus, in contrast to memory devices and electronic circuitry for data
382 storage and processing, which are usually sealed to avoid detrimental environmental effects,
383 sensor technology and transient electronics could benefit directly from the new sensitivity
384 emerging from the interaction between domain walls and point defects. Furthermore, because of
385 mixed ionic-electronic conduction,[146] quasi-dynamical adjustments become possible, separating
386 intrinsic and extrinsic contribution via domain wall displacements. This possibility is illustrated by
387 local conductance measurements on $BiFeO_3$, which showed that conducting features can persist
388 even after 109° domain walls in $BiFeO_3$ have been erased, possibly due to less mobile oxygen
389 vacancies that stay behind.[147] With this, point defects can give a new twist compared to the
390 classical approaches, allowing to spontaneously change the domain wall behavior via the
391 dynamical separation of extrinsic and intrinsic contributions to the electronic response.

392 ***Domain wall functionality in heterostructures.*** Going beyond strain engineering via lattice
393 mismatch or built in-gradients, combinations of interface- and domain-wall-driven effects can be
394 used to create new functionality. For example, structural defects together with lattice mismatch
395 can induce non-switchable ferroelectric domains, leading to the stabilization of extended charged
396 180° head-to-head domain walls in $PbZr_{0.2}Ti_{0.8}O_3$ films grown under ~1.2% biaxial compressive
397 strain.[148] Here, charge compensation at the head-to-head walls is achieved by electrons that are
398 donated by oxygen vacancies near the surface. Alternatively, oxygen vacancies can accumulate
399 directly at such artificially stabilized charged domain walls, giving rise to intriguing quantum
400 phenomena. In seminal work on multiferroic tunnel junctions, it was demonstrated that charged
401 head-to-head walls can be stabilized in $La_{0.7}Sr_{0.3}MnO_3/BaTiO_3/La_{0.7}Sr_{0.3}MnO_3$, leading to resonant
402 tunneling transport as shown in Fig. 2c.[149] The charged wall in the ultrathin ferroelectric $BaTiO_3$ is
403 stabilized by interface dipoles that favor a polarization pointing away from the heterointerfaces
404 (Fig. 2d) and oxygen vacancies which accumulate at the wall. The associated measured reduction

405 of the Ti oxidation state (bulk: Ti^{+4}, wall: $Ti^{+3.95}$) converts into a sheet carrier density of 3×10^{14} cm^{-2}, compensating the domain wall bound charge of about 0.5 C m^{-2}. Electronic confinement within the walls leads to discrete quantum-well energy levels and resonant tunneling, which vanishes along with the domain wall as the $BaTiO_3$ layer is poled into a single domain state. This example demonstrates how domain wall–point defect interactions and interface control can be combined to achieve emergent quantum phenomena, representing a promising strategy towards conceptually new domain-wall based devices.

Novel chemical 2D phases at domain walls. Besides controlling the oxidation state, lattice-mismatch-induced strain and built-in strain gradients at domain walls can be combined to create completely new 2D phases at domain walls. In $TbMnO_3$ films grown on (001)-oriented $SrTiO_3$ (≈5 % lattice mismatch) the domain walls exhibit an unusual structure, where every second Tb atom is replaced by Mn (Fig. 2d).[150] This 2D phase arises from the intense local stress, promoting the formation of domain walls with an artificial chemical structure that is dramatically different from the surrounding bulk. Such control enables a wide range of intriguing design opportunities, manipulating the crystallographic structure, as well as electric, spin and orbital degrees of freedom at domain walls via cation defects in addition to anion defects, i.e., oxygen vacancies and interstitials.

Combining defect chemistry and domain wall engineering thus provides novel opportunities for domain-wall based technology, taking advantages of the strong electronic correlations in oxides and the fundamental impact individual point defects can have on the local electronic structure. In addition, point defects can be used to shape domain walls, affecting their roughness[151,152], as well as the structural and electronic width, and even improve their mobility[133], providing so far largely unexplored opportunities for the utilization of domain wall–point defect interactions.

Improper ferroelectrics for domain wall electronics

Domain walls in improper ferroelectrics. In recent years, there is an increasing interest in improper ferroelectrics where the electric order is not the primary order parameter (BOX 1).[26,27] In this class of materials, ferroelectricity arises as a symmetry-enforced by-product of a structurally or magnetically driven phase transition,[153] which leads to much more flexible boundary conditions regarding the elastic and mechanical compatibility of domain walls than in proper ferroelectrics.[14] As a consequence, a much larger diversity of domain walls spontaneously arises in the as-grown state, offering unconventional functionalities that are not available at proper ferroelectric domain walls. One example for the special nature of improper ferroelectrics is the spontaneous formation of charged 180° domain walls.[50] These charged walls are energetically very unfavorable in proper ferroelectrics,[21] where their formation requires dedicated preparation methods such as electrical trailing fields[154] and frustrated poling[31]. The spontaneous polarization in improper ferroelectrics is typically smaller than in proper ferroelectrics, reaching about 1 $\mu C/cm^2$ in systems with magnetically induced ferroelectricity and 10 $\mu C/cm^2$ in geometric ferroelectrics.[153] Despite the smaller polarization, the domain wall bound charges and associated electrostatic potentials still require electrical screening,[21] driving a variety of intrinsic and extrinsic conduction phenomena.[119] For example, a rough estimation for 180° tail-to-tail walls in improper ferroelectric hexagonal manganites ($P \approx 5.5$ $\mu C/cm^2$) shows that a local charge carrier density of about 6×10^{13} per cm^2 can be expected to appear. In addition to the accumulation and depletion of mobile charge carriers and the respective changes in the electronic transport properties, novel functionalities can arise from the primary structural or magnetic order parameter,[20] including

450 strain- and spin-driven effects, as well as magnetoelectric coupling phenomena, which are
451 discussed below.

452 Analogous to their proper counterparts, improper ferroelectric domain walls are mobile, and it
453 has been demonstrated that they can be injected, moved and erased by electric fields.[49,55,155–157]
454 In addition, domain wall positions and charge states may be manipulated by acting on the primary
455 symmetry breaking order parameter, offering new opportunities for controlling the domain wall
456 response.[158,159] Thus, improper ferroelectrics have several key advantages compared to proper
457 ferroelectrics and generally exhibit higher flexibility to host walls with otherwise energetically
458 unfavorable charge states, explaining the growing interest and expanding research activities
459 related to functional improper ferroelectric domain walls.

460 ***Hexagonal manganites***. Conduction at improper ferroelectric domain walls was discovered in
461 $ErMnO_3$ (Fig. 3a),[50] quickly followed by the observation of conducting walls in $HoMnO_3$[51] and other
462 hexagonal manganites.[53,54,160] During the last decade, the hexagonal manganites evolved into an
463 intensively studied model system for theoretical and experimental domain wall investigations,
464 including both fundamental and application-oriented aspects. The system develops uniaxial
465 improper ferroelectricity below $\approx$ 1400 K due to a coupling to a unit-cell tripling distortive mode,
466 which represents the primary order parameter.[107,161–163] Six symmetry-equivalent structural
467 trimerization domains arise in the ordered state, separated by anti-phase boundaries across which
468 the trimerization phase changes by 60° and the direction of the polarization changes by
469 180°.[49,156,164,165] Wherever domain walls meet, a characteristic six-fold vortex structure is formed
470 which is topologically protected, preventing hexagonal manganites from developing only charge-
471 neutral domain walls.[50,51] Because of this topology-driven phenomenon, both positively and
472 negatively charged domain walls naturally arise in the as-grown state irrespective of their
473 unfavorable electrostatics (Fig. 3a). Driven by the associated electric potentials, the mobile holes
474 in p-type hexagonal manganites redistribute, leading to hole accumulation at negatively charged
475 tail-to-tail walls (enhanced conductivity) and hole depletion at positively charged head-to-head
476 domain walls (reduced conductivity). Intriguingly, the mobility reported for the p-type carriers
477 responsible for the conductivity at the tail-to-tail domain walls in hexagonal manganites is
478 remarkably high ($\approx$ 100 $cm^2 V^{-1} s^{-1}$), i.e., among the highest in oxides, which is essential for good
479 device performance.[79,160] Recently, it was shown that the head-to-head walls can also exhibit
480 higher conductivity than the bulk, but only if sufficiently high electric field are applied to activate
481 the n-type charge carriers at these walls.[101] Differing from proper ferroelectrics, these charged
482 walls are explicitly stable and persist even when their bound charges are not fully screened,
483 representing a rare example of a stable, electronically uncompensated oxide interface.[166,167] While
484 it is still possible to manipulate domain wall positions via, e.g., applied strain,[158] electric
485 fields,[49,155,156,168] and annealing,[169–171] the biggest advantage lies in their stability, which allows
486 using them as robust template for local property engineering.[172,173] Early studies have adopted
487 strategies from semiconductor research changing, e.g., domain wall currents and the electronic
488 domain wall width via aliovalent doping, demonstrating the general possibility to optimize and
489 tailor the response at improper ferroelectric domain walls.[53,54]

490 Aside from the electrostatics-driven intrinsic conductivity at charged domain walls, a wide range
491 of defect-enabled extrinsic effects has been reported for neutral domain walls in hexagonal
492 manganites.[49,50,138,139,174,175] Governed by local strain fields, their conductivity can vary from
493 insulating to conducting, which has been explained based on the segregation enthalpy of oxygen
494 vacancies and interstitials.[135,138,139] In contrast to perovskite materials, oxygen vacancies and
495 interstitials play an equally important role for the electronic transport properties in hexagonal

496 manganites, offering a high flexibility for domain wall engineering via off-stoichiometry.[176–178] In
497 addition, neutral domain walls exhibit enhanced a.c. conductivity at gigahertz frequencies (Fig.
498 3b). The latter was explained based on the excitation of acoustic wave-like domain wall oscillations
499 in the microwave regime and shows the potential to expand domain wall nanoelectronics into the
500 realm of a.c. technology.[72,73] However, the research activities are still on a fundamental level and
501 the majority of the work on hexagonal manganites was performed on the surface of mm-thick
502 single-crystals. Because of this, the impact of the sub-surface domain wall geometry is largely
503 unknown and better control is highly desirable. An important step in this direction are recent
504 investigations on FIB-cut $ErMnO_3$ lamellas (Fig. 3c), facilitating investigations of individual domain
505 walls in well-defined charge states and under more device-relevant geometries in a top-down
506 approach.[179] Recently, the characteristic trimerization domain walls of hexagonal manganites
507 have also been observed in thin films grown by pulsed laser deposition. Here, however, the
508 domain wall transport remains to be measured, which is currently hampered by the small size of
509 the emergent ferroelectric domains.[180,181]

510 ***Hexagonal gallates, indates, and ferrites.*** Although most of the experimental research has been
511 performed on improper ferroelectric domain walls in hexagonal manganites, similar phenomena
512 are expected for a much larger group of isostructural systems, including hexagonal gallates[182] and
513 indates[119], as well as hexagonal ferrites[183,184] and tungsten bronzes[185]. This expectation is justified
514 by different theoretical and experimental investigations, which showed fundamental analogies
515 concerning the formation and structure of ferroelectric domains and domain walls in these
516 systems. Despite the structural similarities, however, different electronic domain walls responses
517 are available, caused by differences in the local chemical environment. For example, DFT
518 calculations showed that while the structure of charged walls are qualitatively similar in all these
519 systems, $InMnO_3$ display wider walls than $YMnO_3$ and $YGaO_3$.[119] Furthermore, stoichiometric
520 $InMnO_3$ and $YGaO_3$ are predicted to display exclusively resistive domain walls because the
521 polarization is too small or the band gap too large, respectively, to introduce the strong band
522 bending necessary for intrinsic electronic conduction at the walls. The theoretical work shows that
523 this larger group of isostructural materials provides an explicitly fertile ground for the exploration
524 of functional domain walls, representing a versatile alternative to the broadly studied perovskite
525 materials. Experimentally, it has already been confirmed using high-angle annular dark field
526 (HAADF) STEM that the hexagonal ferrite, $LuFeO_3$, develops trimerization domain walls similar to
527 hexagonal manganites[186,187] and characteristic six-fold trimerization domains have been resolved
528 in the tungsten bronze $CsNbW_2O_9$ using piezoresponse force microscopy (PFM)[185]. The high
529 chemical flexibility of these hexagonal systems facilitates a wide parameter space for tuning, e.g.,
530 electronic band gaps, carrier density and mobility, as well as the domain wall structure, thereby
531 tailoring the domain wall response on demand. Another possibility is to exploit geometrical
532 confinement effects, exploiting the coupling to the primary symmetry breaking order parameter.
533 This approach was recently applied to control the formation of charged and neutral ferroelectric
534 domain walls via the layer thickness in $LuFeO_3$ superlattices.[187]

535 ***Ruddlesden-Popper perovskites.*** Abundant charged ferroelectric domain walls were also
536 observed in $(Ca,Sr)_3Ti_2O_7$ single-crystals (Fig. 3d), which belong to the Ruddlesden-Popper series
537 of compounds.[56] $(Ca,Sr)_3Ti_2O_7$ is a hybrid improper ferroelectric, which means that a combination
538 of two or more structural order parameters is responsible for the emergence of
539 ferroelectricity.[188,189] Here, it is the combination of a tilting and a rotation of the TiO_6 octahedra
540 that leads to a displacement of the Ca and Sr atoms and, hence, a spontaneous electric
541 polarization of about 4 $\mu C/cm^2$. The complexity of the order parameter coupling in this hybrid
542 improper ferroelectric is reflected at the level of domains, giving rise to the formation of eight

543 types of ferroelectric and four types of ferroelastic walls, including neutral 180° domain walls, as
544 well as conducting head-to-head walls and insulating tail-to-tail walls. This trend is in agreement
545 with the n-type character of oxygen deficient $(Ca,Sr)_3Ti_2O_7$ and can be explained based on the
546 electrostatic potentials associated with the domain wall bound charges. The domain wall
547 conductance varies with the domain wall orientation, but in contrast to the manganites, only
548 discrete orientation angles occur in accordance with the crystallographic symmetry of the system.
549 The results gained on ferroelectric domain walls in the Ruddlesden-Popper perovskite are
550 intriguing as certain members of this family of materials also exhibit giant magnetoresistance[190]
551 and superconductivity[191], i.e., physical properties that potentially also influence the domain wall
552 behaviors with so far unexplored consequences.

553 ***Boracites.*** Another class of improper ferroelectrics with conducting domain walls are the
554 boracites.[55] In boracites, a spontaneous electric polarization of about 1 $\mu C\ cm^{-2}$ arises at the
555 structurally driven paraelectric-to-ferroelectric phase transition (≈ 363 K for $Cu_3B_7O_{13}Cl$)[192],
556 induced by a shearing of the unit cell. In the ferroelectric phase, six different domain states are
557 present, separated by straight domain walls. All fundamental charge configurations are
558 represented, that is, neutral 180° domain walls, as well as positively charged head-to-head and
559 negatively charged tail-to-tail 90° domain walls. Measuring the local transport behavior in
560 $Cu_3B_7O_{13}Cl$, it was shown that the tail-to-tail walls exhibit enhanced conductance, whereas
561 suppressed conductance was observed at head-to-head walls (Fig. 3e), suggesting that conduction
562 is mediated by holes (p-type). Different from the hexagonal manganites, gallates, indates, and
563 ferrites, the domain wall morphology is not governed by topological defects and up to hundreds
564 of micrometers long walls can be created by application of pressure. Furthermore, the conducting
565 tail-to-tail walls can readily be moved by application of an electric field, exhibiting non-trivial
566 dynamics that are currently under investigation with respect to domain-wall enabled negative
567 capacitance.[193]

568 ***Spin-driven ferroelectrics.*** Aside from structural order parameters, magnetic order can break
569 spatial inversion symmetry and induce a spontaneous polarization.[194–196] This effect has been
570 intensively studied in multiferroics and is observed in a wide range of material systems, such as
571 Cr_2BeO_4,[197] $TbMnO_3$,[198] $TbMn_2O_5$,[199] $Ni_3V_2O_8$,[200] $MnWO_4$,[201] CuO,[202] and $DyFeO_3$[203] (for reviews on
572 the topic of spin-driven ferroelectricity, we refer the reader to REFs [204,205]). The strong
573 magnetoelectric coupling in this class of improper ferroelectrics is intriguing as it gives rise to
574 hybrid domain walls with inseparably entangled electric and magnetic degrees of freedom.[206,207]
575 For example, it has been demonstrated that domain walls with charged head-to-head and tail-to-
576 tail section naturally arise in $Mn_{0.95}Co_{0.05}WO_4$.[208] Application of a magnetic field continuously
577 rotates the polarization direction by 90°, converting nominally neutral into charged domain walls
578 and vice versa. Based on LLG simulations, domain wall bound charges with a density up to 10^5 C
579 m^{-3} are expected to arise, allowing deterministic and reversible control of the domain wall charge
580 state. A similar effect was observed in $TbMnO_3$, where neutral domain walls were converted into
581 charged head-to-head and tail-to-tail walls, exploiting a magnetic-field induced first-order phase
582 transition across which the direction of the improper ferroelectric polarization changes by 90°.[209]
583 This cross-coupling of electric and magnetic degrees of freedom facilitates novel device-concepts
584 based on magnetoelectric domain walls as discussed below.

585

586

Domain walls becoming the device

The expansion of domain wall research towards materials with improper ferroelectricity has revealed a multitude of unusual types of walls with advanced functional properties that are not available at conventional proper ferroelectric domain walls. These discoveries have triggered a conceptually new approach for developing domain-wall based nanotechnology: In contrast to the classical approach, which relies on the creation and deletion of ferroelectric domain walls within a much larger device architecture, the new idea is to use individual domain walls to emulate the behavior of electronic components, turning the domain walls themselves into devices.

Reversible electric-field control of domain wall resistivity. Building on the idea to utilize intrinsic domain wall properties to control and process electronic signals, the response at different types of improper ferroelectric domain walls in hexagonal manganites has been exploited to mimic digital switches[101] and achieve diode-like behavior[138] at the nanoscale. In general, the density of domain walls in hexagonal manganites can be adjusted via the cooling rate across the ferroelectric phase transition at high temperature ($\gtrsim$ 1000 K).[169–171] Domain walls can be created and moved by application of sufficiently high electric fields ($\approx$ 100 kV/cm at 120 K),[49,155,156] thus offering the same spatial degrees of freedom as proper ferroelectrics. However, when operated at room-temperature and low voltage, the domain walls are extraordinarily stable,[50,166] representing stationary 2D objects with unique functional properties. It was demonstrated that the current at head-to-head domain walls in $ErMnO_3$ can be reversibly switched between resistive and conductive behavior by application of a gate-voltage in the order of 1 to 3 V,

realizing a domain-wall-based binary switch (Fig. 4a).[101] The transition from resistive to conductive behavior arises because of the pronounced band bending at the head-to-head walls in $ErMnO_3$, which leads to the formation on an electronic inversion layer. At low voltage, conduction at the walls is hole-dominated (resistive, p-type),[50,79] whereas electrons dominate the conductance at higher voltages (conductive, n-type), reflecting a qualitative change in the transport behavior.

Diode-like behavior at electrode–domain wall junctions. Another opportunity is to utilize the specific electronic properties at domain walls in combination with different electrode materials to exploit the local nature of emergent contact phenomena, pushing related applications to ultra-small length scales. One example is the observation of distinct diode-like properties at neutral domain walls in $ErMnO_3$ which occur at the electrode-wall junction and facilitate alternating-to-direct current conversion (Fig. 4b).[138] Due to the enhanced conductance of the neutral domain walls, higher frequencies are required to short-circuit the Schottky-barrier at the electrode-wall junction compared to the bulk, enabling operation as half-wave rectifiers in the kilo- to megahertz range. Thus, going beyond standard metal–semiconductor junctions and domain-specific rectification in ferroelectrics[210], the utilization of domain walls could lead to nano-sized diodes with lateral dimensions defined by the smallest achievable contact area.

Magnetic control of domain wall charge states. Aside from domain walls in geometrically driven improper ferroelectrics, application opportunities for hybrid electric/magnetic domain walls have been discussed.[208,209] The studies, however, are still on a very fundamental level, focusing on proof-of-concept experiments under laboratory conditions at cryogenic temperature. The possibility to reversibly change the domain wall charge state (abruptly or continuously) suggests that the polarization charge may be used as quasi-dopant to control the electronic transport behavior at ferroelectric domain walls.[154] The advantage of the hybrid electric/magnetic domain walls compared to proper ferroelectric domain walls is that their charge state can be controlled by magnetic fields even after the material has been implemented into a device, enabling the

632 design of magnetoelectric domain wall transistors as sketched in Fig. 4c. Furthermore, it has been
633 demonstrated that neutral, as well as charged head-to-head and tail-to-tail domain walls in
634 $TbMnO_3$ can be written optically using a laser (continuous wave or pulsed),[211] opening new
635 possibilities for optical engineering of functional domain wall patterns and networks. At present,
636 the small polarization values and cryogenic temperatures associated with magnetically induced
637 ferroelectricity are clearly incompatible with technological applications and the electronic
638 conduction at the hybrid magnetic/electric domain walls is yet to characterized. However, the
639 development of systems with larger spontaneous polarization and ordering temperatures closer
640 to room-temperature is well on the way,[212–215] so that domain walls in magnetically induced
641 improper ferroelectrics may play an increasingly important role in the future.

642

643 ## Conclusion and perspective

644 The idea of developing electronic devices based on ferroelectric domain walls has been inspiring
645 researchers for the past 50 years.[28] The recent development in materials synthesis, advanced
646 imaging techniques and simulations drastically improved our understanding of the complex
647 nanoscale physics and facilitate the creation of first proof-of-concept devices, where resistive
648 states are set by injecting, repositioning, and deleting domain walls.[11,18–24] The main challenges of
649 this classical approach nowadays relate to materials engineering, concerning technological needs
650 such as larger on/off rations, enhanced current densities, and endurance. Another aspect that is
651 attracting increasing attention is the 3D corrugation of domain walls[179,216–218] and its impact on the
652 electronic properties. Because of the one-to-one correlation between domain wall orientation
653 and charge state, their electronic response can readily be reconfigured by changing the inclination
654 angle relative to the polarization direction. Thus, by gradually changing the domain wall
655 orientation, a continuous set of resistance states can be realized, enabling innovative
656 technologies, such as multilevel data storage and the development of domain-wall based synaptic
657 devices.[61] Individual memristive domain walls, for example, could replicate key properties of
658 biological synapses and serve as building blocks for neuromorphic circuitry, offering much smaller
659 feature size than device architectures relying on ferroelectric domains.

660 Progress is mainly limited by the challenges associated with the imaging of ferroelectric domain
661 walls in 3D. Optical methods allow for 3D tomography studies of the average domain wall
662 structure at the micrometer length scale, but do not resolve the nanoscale features that
663 determine the electronic response. Here, the research will strongly benefit from the ongoing
664 advances in 3D microscopy methods, such as dark-field X-ray microscopy[219], as well as FIB-SEM[220]
665 and atom-probe tomography[221], establishing new physics and functionalities that originate from
666 local variations in, e.g., the curvature, width and roughness. Linear-scaling DFT codes like
667 CONQUEST[222] may assist the microscopy studies, enabling explicit DFT calculations on supercells
668 with several thousand atoms and, hence, more realistic calculations of the domain wall structure
669 in 3D.[182]

670 First studies of dynamical phenomena in the microwave regime suggest new application
671 opportunities for ferroelectric domain walls in devices for radio-frequency applications, expanding
672 the domain wall nanoelectronics into the realm of a.c. technology. However, while anomalous
673 microwave a.c. conductivity has been observed at neutral domain walls, detailed knowledge about
674 their charged counterparts remains elusive. In particular, a gap remains in the understanding of
675 the adiabatic response of ferroelectric domain walls in the sub-microwave regime, which is
676 relevant for low-frequency a.c. electronics components enabling, e.g., domain-wall based

capacitors for charge storage, as well as inductors and transformers. Aside from the electronic properties of ferroelectric domain walls, unusual domain wall–phonon interactions have been reported that may be used to control heat flux[91] and it was demonstrated that the walls are mechanically softer than the surrounding domains, providing mechanical contrast that could simplify the read-out of ferroelectrically stored information[87].

Defect–domain wall interactions, while addressed in a growing number of studies, need to be tackled in a systematic way to understand and utilize the underlying nanoscale physics in device applications. For example, the combined sensitivity of ferroelectric oxides to the surrounding atmosphere[223] and the propensity for point defects to form at certain domain walls makes ferroelectric walls excellent candidates for nanoscale environmental sensors. Due to self-diffusion and electromigration, ferroelectric domain walls can act as a sink for oxygen defects. The latter locally promotes either p-type (interstitials) or n-type (vacancies) behavior, converting environmental changes in oxygen atmosphere into an electronic signal. Point defects may also be used to create gradients and, hence, flexoelectric,[224,225] rotopolar and trilinear couplings[226] that contribute to the polarization at the domain walls. Furthermore, they are predicted to induce new functional properties not available in stoichiometric systems leading, for instance, to a spontaneous magnetization at ferroelectric domain walls in an otherwise non-magnetic material[227]. In general, spin-dependent transport properties and cross-correlations between electric and magnetic degrees of freedom at ferroelectric domain walls will require more research to go beyond just conductivity and access emergent magnetoresistance[84–86] and multiferroic phenomena for spintronics applications[228].

The idea to utilize intrinsic physical properties at stationary ferroelectric domain walls to control electrical currents and emulate the behavior of electronic components – instead of controlling conductivity by injecting and erasing walls – offers exciting opportunities for nanotechnology. In particular, this strategy has the potential to fully capitalize the ultra-small feature size of domain walls and enable low-power operation, breaking the mould of classical device architectures. Clearly, more work is needed to establish a fundamental understanding and the physical limits before domain walls can replace electronic components, but first proof-of-concept studies on improper ferroelectric domain walls already showed the general feasibility of the approach[101,138]. Here, the dream would be to eventually achieve adaptable domain-wall circuitry, where components may be created, reorganized, optimized or updated during the whole lifetime of a system, going towards adaptable nanoelectronics.

In conclusion, is clear that exciting times are lying ahead of us regarding the research on functional ferroelectric domain walls. Novel possibility are arising at a remarkable speed, including domain-wall-inspired heterostructures,[229] control via confinement effects in multilayers,[187] and the manipulation of domain walls in free-standing thin films[230]. Thus, within only 10 years, the field has evolved way beyond the original ideas and world-wide activities are still on the rise, potentially revolutionizing nanotechnology in the years to come.

Acknowledgements - D.M. acknowledges funding from the European Research Council (ERC) under the European Union's Horizon 2020 Research and Innovation Programme (Grant Agreement No. 863691). The Research Council of Norway (RCN) partly supported this work through the Norwegian Micro and Nano-Fabrication Facility, NorFab (Project No. 295864) and its Centres of Excellence funding scheme, project number 262633, "QuSpin". S.M.S. and D.M. were further supported by the RCN via the FRIPRO projects 231430 and 263228, respectively.

722 **FIGURES AND CAPTIONS**

723

724

725

726

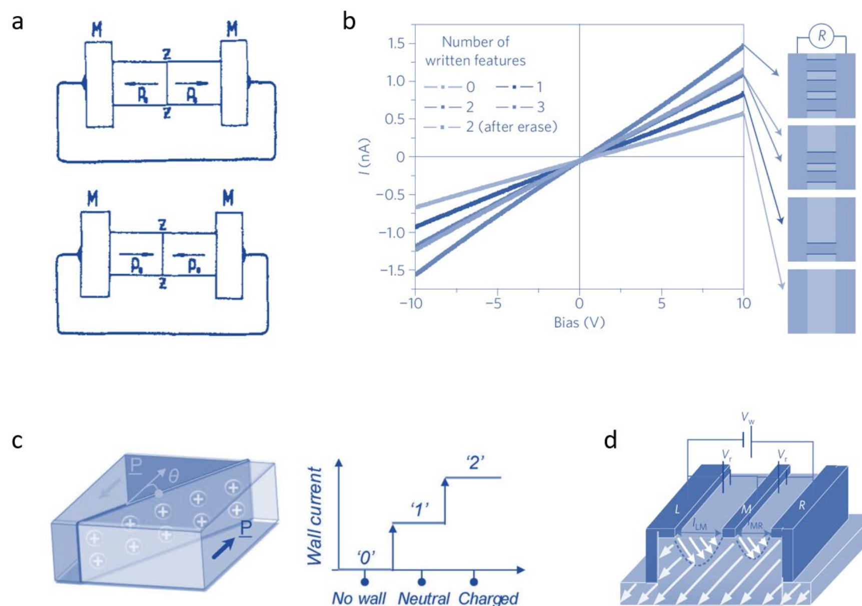

727

728 **Figure 1 | Classical concepts for domain wall based nanoelectronics. a**, Original concept for
729 controlling conductivity based on charged domain walls, using a ferroelectric mounted between
730 two metal electrodes (M). Due to the redistribution of mobile charge carriers, the tail-to-tail
731 (upper panel) and head-to-head (lower panel) walls were expected to show enhanced electron
732 and hole conductivity, respectively. Panel **a** adapted with permission from REF [28]. **b**, Multi-level
733 resistance control based on conducting ferroelectric domain walls in $BiFeO_3$. The number of
734 ferroelectric domain walls between two electrodes determines the I(V)-characteristics, enabling
735 reversible control via the creation and deletion of domains. Panel **b** reproduced with permission
736 from REF [25]. **c**, Concept of a tri-state domain wall memory, utilizing the observation that the
737 domain wall charge state in $BiFeO_3$ can be manipulated. In the proposed two-terminal device,
738 the three states correspond to no domain wall ('0'), a neutral domain wall ('1'), and a charged
739 domain wall ('2') between the electrodes. Panel **c** adapted with permission from REF [60]. **d**,
740 Domain-wall assisted read-out in ferroelectric memory devices. Depending on the underlying
741 domain configuration, partial switching can create highly conducting domain walls, enabling
742 non-destructive read-out of the polarization state via transient electrical currents. Panel **d**
743 adapted with permission from REF [69].

744

745

746

747

748

749

750

751

752

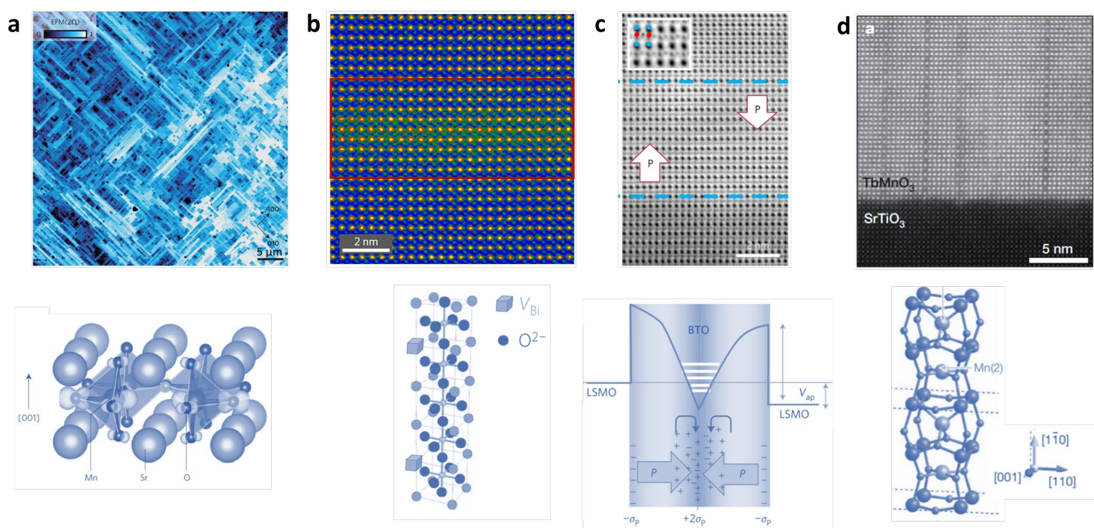

753

754 **Figure 2 | Functionality enabled by domain wall–point defect interactions. a**, Conductance map
755 showing stripe-like nano-arrays with varying conductance in a strained $SrMnO_3$ film (bright: high
756 conductivity, dark: low conductivity). The different arrays are separated by polar domain walls at
757 which oxygen vacancies accumulate, acting as a barrier for the electronic transport. The lower
758 panel shows the calculated local structure around an oxygen vacancy. Panel **a**
759 adapted/reproduced with permission from REF [141]. **b**, Low-angle annular dark field (LAADF) STEM
760 image of a 109° domain wall in $BiFeO_3$. Colors indicate the lattice-strain around the domain wall,
761 correlating with the accumulation of Bi vacancies charge compensated by Fe^{4+} ions. The
762 schematic visualizes the presence of point defects at the domain wall, showing Bi vacancies as
763 blue boxes. Panel **b** adapted/reproduced with permission from REF [100]. **c**, Cross-sectional data of
764 a $La_{0.7}Sr_{0.3}MnO_3/BaTiO_3$ superlattice (fast Fourier transform filtered annular bright-field image),
765 showing the lattice position of oxygen (grey), Ti (red), and Ba (blue). A head-to-head domain wall
766 is present in the middle of the $BaTiO_3$ layer as shown by the white arrows, which indicate the
767 direction of the polarization *P*. The voltage-dependent band banding and discrete quantum-well
768 energy levels that arise due to electronic confinement within the walls is sketched in the lower
769 part of **c**. Panel **c** adapted/reproduced with permission from REF [149]. **d**, High-angle annular dark
770 field (HAADF) STEM image of a strained $TbMnO_3$ film on $SrTiO_3$. Darker lines correspond to
771 domain walls, where Mn atoms substitute for Tb atoms, leading to a new chemical phase as
772 sketched in the lower part. Panel **d** adapted/reproduced with permission from REF [150].

773

774

775

776

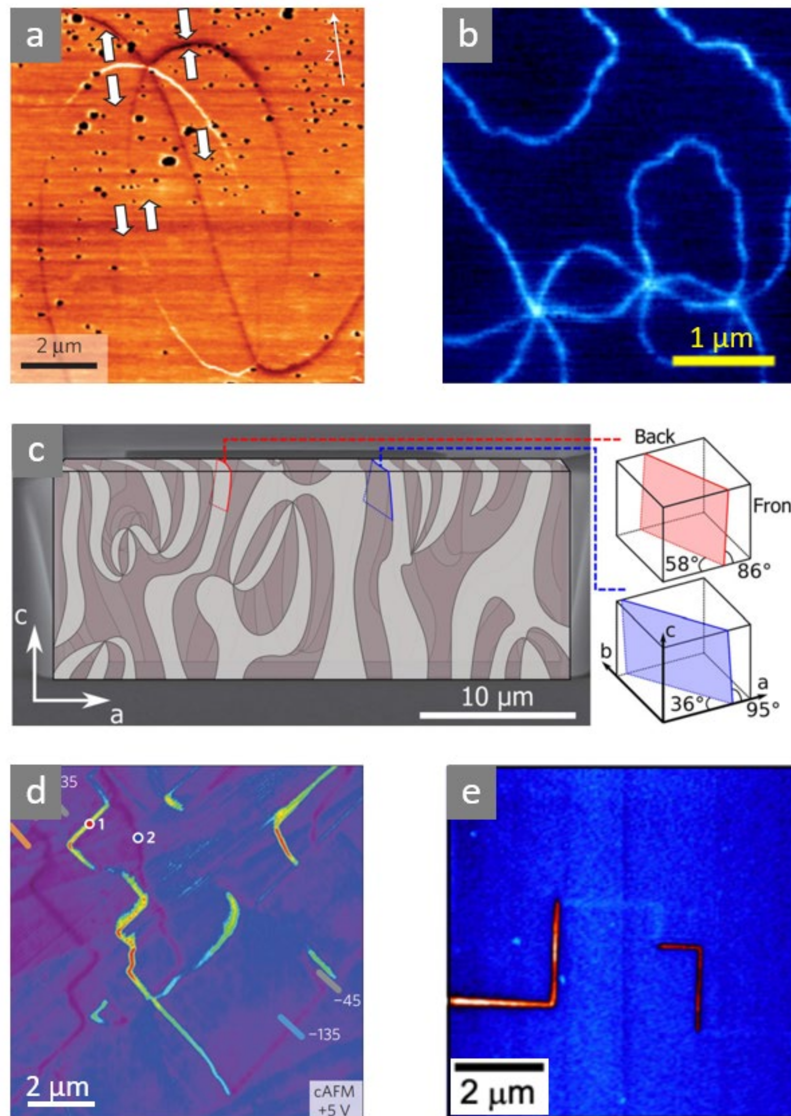

777

778 **Figure 3 | Conducting domain walls in improper ferroelectrics. a**, Direct-current (d.c.)
779 conductance map gained on an $ErMnO_3$ single crystal, revealing anisotropic electronic transport
780 properties at the ferroelectric 180° domain walls. Tail-to-tail domain walls exhibit enhanced p-
781 type conductance (bright), whereas suppressed conductance is observed at the head-to-head
782 walls (dark). Polarization directions are indicated by the arrows. Panel **a** reproduced with
783 permission from REF [50]. **b**, Scanning impedance microscopy image recorded on $ErMnO_3$ with out-
784 of-plane polarization at 1 GHz. The data reveals a pronounced response at the neutral domain
785 walls, which has been attributed to the excitation of domain-wall oscillations at terahertz
786 frequencies. Panel **b** adapted with permission from REF [72]. **c**, Scanning electron microscopy
787 image of a FIB-cut lamella, extracted from an $ErMnO_3$ single crystal (thickness ≈ 700 nm). Colors
788 indicate 180° domains of opposite ferroelectric polarization (in-plane *P*). Panel **c** reproduced
789 with permission from REF [179]. **d**, Conductive atomic force microscopy image showing enhanced
790 d.c. conductance at head-to-head domain walls (bright) in a $Ca_{2.46}Sr_{0.54}Ti_2O_{7-\delta}$ crystal. Panel **d**
791 reproduced with permission from REF [56]. **e**, Conductance map gained on a $Mg_3B_7O_{13}Cl$ single
792 crystal. Increased electronic d.c. conductance (bright) is measured at the
793 ferroelectric/ferroelastic tail-to-tail domain walls. Panel **e** reproduced with permission from REF
794 [55].

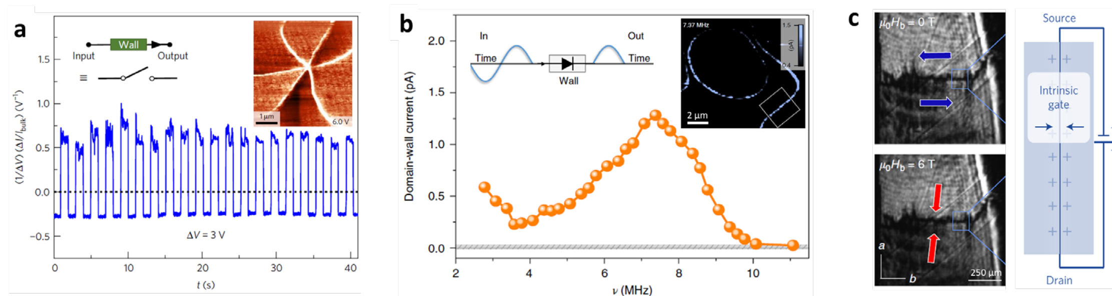

Figure 4 | Emulating the behavior of electronic components based on ferroelectric domain walls. a, Reversible switching between resistive (p-type) and conducting (n-type) behavior at a head-to-head domain wall in $ErMnO_3$. The cAFM scan in the inset is gained at 6V, that is, in the regime where both tail-to-tail and head-to-head walls exhibit enhanced conductance. Panel **a** adapted with permission from REF [101]. **b**, Frequency-dependent half-wave rectification at neutral ferroelectric domain walls in $ErMnO_3$. The spectrum reveals that for frequencies below ≈ 10 MHz, a.c. currents are rectified at the electrode-wall junction. Inset: AC-cAFM map recorded at 7.37 MHz, showing the domain wall area across which the spectrum is averaged. Panel **b** adapted with permission from REF [138]. **c**, Magnetic-field control of the ferroelectric domain wall state in multiferroic $Mn_{0.95}Co_{0.05}WO_4$. By application of a magnetic field, the nominally neutral side-by-side domain wall (H = 0 T) is transformed into a head-to-head domain wall (H = 6 T). Conceptually, the configurational change enables the design of domain-wall-based two-terminal field-effect transistors, where the polarization charges play the role of the gate as the sketch illustrates. Panel **c** reproduced and adapted with permission from REFs [208] and [101], respectively.

Box 1 | | Types of ferroelectric order and domain walls

Primary ferroics

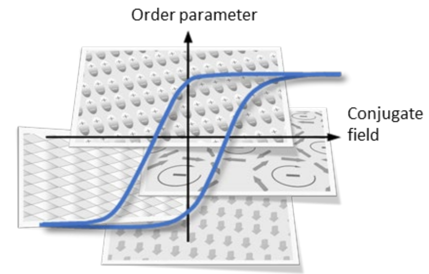

In primary ferroic materials, elastic, electric, magnetic, or toroidic order arises spontaneously across a non-disruptive phase transition, breaking one or more point-symmetry operations.[231,232] The associated ferroelastic, -electric, -magnetic, or -toroidic order parameter of the transition can point in a least two symmetry-equivalent directions, giving rise to the formation of domains. The order parameter is uniform within the domains and changes orientation across the domain walls. Application of a conjugate field can switch the order parameter between symmetry-equivalent orientations, enabling control of domains and domain states. The number of different domains is equal to the number of symmetry-equivalent order parameter orientations, which is given by the ratio of symmetry operations in the point groups of the high-temperature para-phase and the low-temperature ferroic phases.

Proper and improper ferroelectrics

Proper displacive ferroelectricity

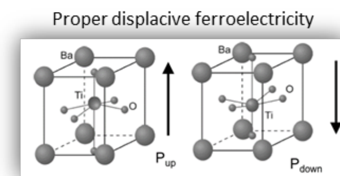

Structurally driven improper ferroelectricity

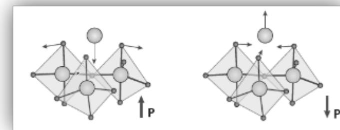

Magnetically driven ferroelectricity

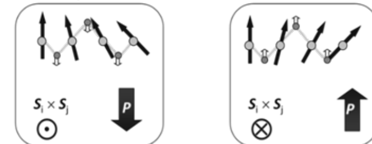

In proper ferroelectrics, the electric polarization is the primary symmetry-breaking order parameter, driving the phase transition from the disordered paraelectric phase to the ordered ferroelectric state.[14] Examples of proper ferroelectrics are the perovskites $BaTiO_3$, $LiNbO_3$, and $PbZr_xTi_{1-x}O_3$ (PZT). Here, displacements of cations with respect to the anion sublattice give rise to electric dipoles. In these prototypical displacive ferroelectrics, ion displacements are stabilized by partial covalency between O^{2-} anions and d^0 cations such as Ti^{4+} or Nb^{5+}.

In improper ferroelectrics, the primary symmetry-breaking order parameter is not the electric polarization.[26,27,233] Ferroelectricity arises as a secondary effect of the symmetry-breaking caused by a magnetic or structural instability. Typical examples of structurally driven improper ferroelectrics are $Gd_2(MoO_4)_3$ and $YMnO_3$.[107,234] Magnetically induced ferroelectricity is observed, e.g., in $TbMnO_3$, $MnWO_4$ and $Ni_3V_2O_8$, facilitating a strong coupling between the charge and spin degrees of freedom.[198,200,201]

Neutral and charged domain walls

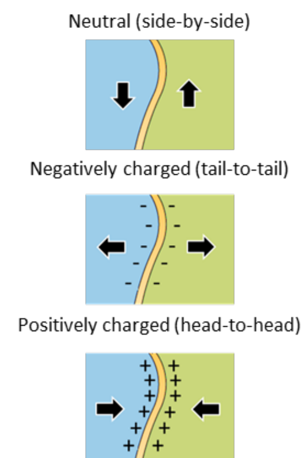

The relative orientation of the order parameter across the domain wall determines the local domain-wall charge state. At neutral walls, the polarization vectors of the two domains are arranged side-by-side with div $P = 0$ across the wall. Thus, the net charge is zero, which avoids the build-up of an energetically costly electrostatic field. In contrast, a non-zero density of bound domain-wall charges occurs at head-to-head and tail-to-tail domain walls (div $P = \pm\rho_{bound}$). The associated electrostatic potential requires screening, driving a redistribution of mobile charge carriers (electronic and/or ionic) within the material.[32,33] For example, in ferroelectric p-type semiconductors, electron holes tend to accumulate at the negatively charged tail-to-tail domain walls and deplete at positively charged head-to-head domain walls, leading to locally enhanced and reduced conductivity, respectively.[50] In reality, however, ferroelectric domain walls are not perfectly flat; point defects, for instance, can induce local bending, and domain walls may gradually change orientation along their way, leading to mixed-type ferroelectric domain walls.[104]

Box 2 | **Point defects and domain walls**

Point defects

Point defects are zero-dimensional lattice imperfections, such as vacancies, interstitials, dopants and impurities. The defect locally changes the material`s symmetry and, hence, can have significant impact on the electronic, magnetic and orbital properties. In metal oxides, the concentration of vacancies or interstitials can be very high, exceeding 30% in some materials.[223,235] However, for concentrations larger than 1-10%, the term nonstoichiometry is more descriptive as electronic states and/or strain fields around point defects interact, leading to new phenomena and collective effects.

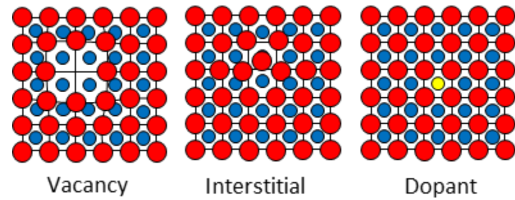

Concentration and mobility

At finite temperatures, point defects are always present in real materials.[236] Their equilibrium concentration is given by the balance between enthalpy cost and entropy gain of defect formation, and increases exponentially with temperature. In addition, the concentration depends on atmospheric conditions, e.g., for metal oxides on the partial pressure of oxygen, following le Chatelier`s principle. In metal oxides, it is useful to distinguish between oxygen defects (vacancies and interstitials) and metal cation defects. The oxygen defects can arise post-growth and are, in principle, reversible. In contrast, cation defects usually form irreversibly at high temperatures during synthesis. The rationale for this division is that oxygen defects generally have much higher mobility than cation defects and can be readily exchanged with the surrounding atmosphere. To engineer the physical properties that originate from the interaction of point defects with domain walls, such as extrinsic conduction contributions and spatial mobility, non-equilibrium concentrations can be frozen in, for example via annealing and quenching from an elevated temperature.[237,238]

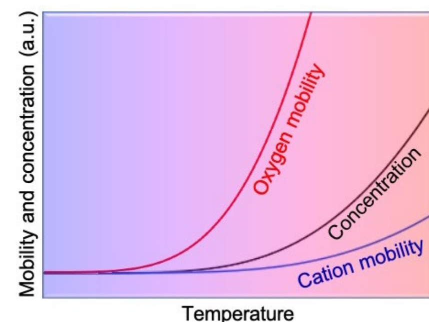

Accumulation, depletion and pinning

Both point defects and domain walls are surrounded by local strain fields that arise due to the broken symmetry. In general, a material can lower its energy by co-locating point defects and domain walls that exhibit similar local lattice strain, maximizing the volume of unperturbed bulk material.[133] The latter explains the strain-driven accumulation of point defects observed at neutral ferroelectric domain walls.[138] Conversely, domain walls tend to get pinned by defects that exhibit compatible local strain. Point defects with incompatible local strain have the opposite effect, leading to a depletion at domain walls[135] and possibly enhanced domain wall mobility.[136] At charged ferroelectric domain walls, the screening of the electrostatic potential creates an additional driving force for the redistribution of charged point defects. For example, positively charged oxygen vacancies will have a propensity for accumulating at negatively charged tail-to-tail walls. Vice versa, the electrostatic potential drives a depletion of unfavorably charged point defects, e.g., leading to a depletion of oxygen vacancies at head-to-head walls.

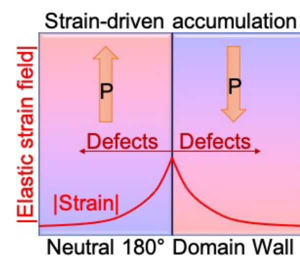

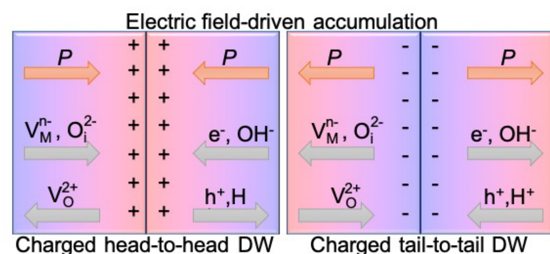

923 **References**
924

925 1. Mannhart, J. & Schlom, D. G. Oxide Interfaces—An Opportunity for Electronics. *Science* **327**,
926 1607–1611 (2010).
927 2. Hwang, H. Y. *et al.* Emergent phenomena at oxide interfaces. *Nat. Mater.* **11**, 103–113 (2012).
928 3. Kroemer, H. Nobel Lecture: Quasielectric fields and band offsets: teaching electrons new tricks.
929 *Rev. Mod. Phys.* **73**, 783–793 (2001).
930 4. The interface is still the device. *Nat. Mater.* **11**, 91–91 (2012).
931 5. Ziese, M. & Thornton, M. J. *Spin Electronics*. (Springer-Verlag, 2001).
932 6. Back, C. *et al.* The 2020 skyrmionics roadmap. *J. Phys. Appl. Phys.* **53**, 363001 (2020).
933 7. Varignon, J., Vila, L., Barthélémy, A. & Bibes, M. A new spin for oxide interfaces. *Nat. Phys.* **14**,
934 322–325 (2018).
935 8. Fert, A., Reyren, N. & Cros, V. Magnetic skyrmions: advances in physics and potential applications.
936 *Nat. Rev. Mater.* **2**, 1–15 (2017).
937 9. Stemmer, S. & James Allen, S. Two-Dimensional Electron Gases at Complex Oxide Interfaces.
938 *Annu. Rev. Mater. Res.* **44**, 151–171 (2014).
939 10. Ramesh, R. & Schlom, D. G. Creating emergent phenomena in oxide superlattices. *Nat. Rev.*
940 *Mater.* **4**, 257–268 (2019).
941 11. Meier, D., Seidel, J., Gregg, M. & Ramesh, R. *Domain Walls: From Fundamental Properties to*
942 *Nanotechnology Concepts*. (Oxford University Press, 2020).
943 12. Aird, A. & Salje, E. K. H. Sheet superconductivity in twin walls: experimental evidence of. *J.*
944 *Phys. Condens. Matter* **10**, L377–L380 (1998).
945 13. Aird, A., Domeneghetti, M. C., Mazzi, F., Tazzoli, V. & Salje, E. K. H. Sheet superconductivity
946 in : crystal structure of the tetragonal matrix. *J. Phys. Condens. Matter* **10**, L569–L574 (1998).
947 14. Tagantsev, A., Cross, L. E. & Fousek, J. *Domains in Ferroic Crystals and Thin Films*. (Springer-
948 Verlag, 2010).

949 15. Salje, E. K. H. Multiferroic Domain Boundaries as Active Memory Devices: Trajectories
950 Towards Domain Boundary Engineering. *ChemPhysChem* **11**, 940–950 (2010).
951 16. Aert, S. V. *et al.* Direct Observation of Ferrielectricity at Ferroelastic Domain Boundaries in
952 $CaTiO_3$ by Electron Microscopy. *Adv. Mater.* **24**, 523–527 (2012).
953 17. Geng, Y., Lee, N., Choi, Y. J., Cheong, S.-W. & Wu, W. Collective Magnetism at Multiferroic
954 Vortex Domain Walls. *Nano Lett.* **12**, 6055–6059 (2012).
955 18. Nataf, G. F. *et al.* Domain-wall engineering and topological defects in ferroelectric and
956 ferroelastic materials. *Nat. Rev. Phys.* 1–15 (2020) doi:doi.org/10.1038/s42254-020-0235-z.
957 19. Catalan, G., Seidel, J., Ramesh, R. & Scott, J. F. Domain wall nanoelectronics. *Rev. Mod. Phys.*
958 **84**, 119–156 (2012).
959 20. Meier, D. Functional domain walls in multiferroics. *J. Phys. Condens. Matter* **27**, 463003
960 (2015).
961 21. Bednyakov, P. S., Sturman, B. I., Sluka, T., Tagantsev, A. K. & Yudin, P. V. Physics and
962 applications of charged domain walls. *Npj Comput. Mater.* **4**, 65 (2018).
963 22. Sharma, P., Schoenherr, P. & Seidel, J. Functional Ferroic Domain Walls for Nanoelectronics.
964 *Materials* **12**, (2019).
965 23. Evans, D. M., Garcia, V., Meier, D. & Bibes, M. Domains and domain walls in multiferroics.
966 *Phys. Sci. Rev.* **5**, (2020).
967 24. Jiang, A. Q. & Zhang, Y. Next-generation ferroelectric domain-wall memories: principle and
968 architecture. *NPG Asia Mater.* **11**, 2 (2019).
969 25. Seidel, J. *et al.* Conduction at domain walls in oxide multiferroics. *Nat. Mater.* **8**, 229–234
970 (2009).
971 26. Dvořák, V. Improper ferroelectrics. *Ferroelectrics* **7**, 1–9 (1974).
972 27. Levanyuk, A. P. & Sannikov, D. G. Improper ferroelectrics. *Sov. Phys. Uspekhi* **17**, 199 (1974).
973 28. Vul, B. M., Guro, G. M. & Ivanchik, I. I. Encountering domains in ferroelectrics. *Ferroelectrics*
974 **6**, 29–31 (1973).

975 29. Merz, W. J. Double Hysteresis Loop of $BaTiO_3$ at the Curie Point. *Phys. Rev.* **91**, 513–517
976 (1953).
977 30. Sluka, T., Tagantsev, A. K., Damjanovic, D., Gureev, M. & Setter, N. Enhanced
978 electromechanical response of ferroelectrics due to charged domain walls. *Nat. Commun.* **3**, 748
979 (2012).
980 31. Sluka, T., Tagantsev, A. K., Bednyakov, P. & Setter, N. Free-electron gas at charged domain
981 walls in insulating $BaTiO_3$. *Nat. Commun.* **4**, 1808 (2013).
982 32. Eliseev, E. A., Morozovska, A. N., Svechnikov, G. S., Gopalan, V. & Shur, V. Ya. Static
983 conductivity of charged domain walls in uniaxial ferroelectric semiconductors. *Phys. Rev. B* **83**,
984 235313 (2011).
985 33. Gureev, M. Y., Tagantsev, A. K. & Setter, N. Head-to-head and tail-to-tail 180° domain walls
986 in an isolated ferroelectric. *Phys. Rev. B* **83**, 184104 (2011).
987 34. Bihan, R. L. Study of ferroelectric and ferroelastic domain structures by scanning electron
988 microscopy. *Ferroelectrics* **97**, 19–46 (1989).
989 35. Aristov, V. V., Kokhanchik, L. S. & Voronovskii, Y. I. Voltage contrast of ferroelectric domains
990 of lithium niobate in SEM. *Phys. Status Solidi A* **86**, 133–141 (1984).
991 36. Schröder, M. *et al.* Conducting Domain Walls in Lithium Niobate Single Crystals. *Adv. Funct.*
992 *Mater.* **22**, 3936–3944 (2012).
993 37. Werner, C. S. *et al.* Large and accessible conductivity of charged domain walls in lithium
994 niobate. *Sci. Rep.* **7**, 9862 (2017).
995 38. Seidel, J. *et al.* Domain Wall Conductivity in La-Doped $BiFeO_3$. *Phys. Rev. Lett.* **105**, 197603
996 (2010).
997 39. Farokhipoor, S. & Noheda, B. Conduction through 71° Domain Walls in $BiFeO_3$ Thin Films.
998 *Phys. Rev. Lett.* **107**, 127601 (2011).
999 40. Zhang, Y. *et al.* Intrinsic Conductance of Domain Walls in $BiFeO_3$. *Adv. Mater.* **31**, 1902099
1000 (2019).

1001 41. Maksymovych, P. *et al.* Dynamic Conductivity of Ferroelectric Domain Walls in $BiFeO_3$. *Nano*
1002 *Lett.* **11**, 1906–1912 (2011).
1003 42. Chiu, Y.-P. *et al.* Atomic-Scale Evolution of Local Electronic Structure Across Multiferroic
1004 Domain Walls. *Adv. Mater.* **23**, 1530–1534 (2011).
1005 43. Vasudevan, R. K. *et al.* Domain Wall Geometry Controls Conduction in Ferroelectrics. *Nano*
1006 *Lett.* **12**, 5524–5531 (2012).
1007 44. Guyonnet, J., Gaponenko, I., Gariglio, S. & Paruch, P. Conduction at Domain Walls in
1008 Insulating $Pb(Zr_{0.2}2Ti_{0.8})O_3$ Thin Films. *Adv. Mater.* **23**, 5377–5382 (2011).
1009 45. Gaponenko, I., Tückmantel, P., Karthik, J., Martin, L. W. & Paruch, P. Towards reversible
1010 control of domain wall conduction in $Pb(Zr_{0.2}2Ti_{0.8})O_3$ thin films. *Appl. Phys. Lett.* **106**, 162902
1011 (2015).
1012 46. Maksymovych, P. *et al.* Tunable Metallic Conductance in Ferroelectric Nanodomains. *Nano*
1013 *Lett.* **12**, 209–213 (2012).
1014 47. Stolichnov, I. *et al.* Bent Ferroelectric Domain Walls as Reconfigurable Metallic-Like
1015 Channels. *Nano Lett.* **15**, 8049–8055 (2015).
1016 48. Lindgren, G. & Canalias, C. Domain wall conductivity in $KTiOPO_4$ crystals. *APL Mater.* **5**,
1017 076108 (2017).
1018 49. Choi, T. *et al.* Insulating interlocked ferroelectric and structural antiphase domain walls in
1019 multiferroic $YMnO_3$. *Nat. Mater.* **9**, 253–258 (2010).
1020 50. Meier, D. *et al.* Anisotropic conductance at improper ferroelectric domain walls. *Nat. Mater.*
1021 **11**, 284–288 (2012).
1022 51. Wu, W., Horibe, Y., Lee, N., Cheong, S.-W. & Guest, J. R. Conduction of Topologically
1023 Protected Charged Ferroelectric Domain Walls. *Phys. Rev. Lett.* **108**, 077203 (2012).
1024 52. Du, Y. *et al.* Domain wall conductivity in oxygen deficient multiferroic $YMnO_3$ single crystals.
1025 *Appl. Phys. Lett.* **99**, 252107 (2011).

1026 53. Schaab, J. *et al.* Optimization of Electronic Domain-Wall Properties by Aliovalent Cation
1027 Substitution. *Adv. Electron. Mater.* **2**, 1500195 (2016).
1028 54. Holstad, T. S. *et al.* Electronic bulk and domain wall properties in B-site doped hexagonal
1029 $ErMnO_3$. *Phys. Rev. B* **97**, 085143 (2018).
1030 55. McQuaid, R. G. P., Campbell, M. P., Whatmore, R. W., Kumar, A. & Gregg, J. M. Injection and
1031 controlled motion of conducting domain walls in improper ferroelectric Cu-Cl boracite. *Nat.*
1032 *Commun.* **8**, 15105 (2017).
1033 56. Oh, Y. S., Luo, X., Huang, F.-T., Wang, Y. & Cheong, S.-W. Experimental demonstration of
1034 hybrid improper ferroelectricity and the presence of abundant charged walls in $(Ca,Sr)_3Ti_2O_7$
1035 crystals. *Nat. Mater.* **14**, 407–413 (2015).
1036 57. Holstad, T. S. *et al.* Application of a long short-term memory for deconvoluting conductance
1037 contributions at charged ferroelectric domain walls. *Npj Comput. Mater.* **6**, 1–7 (2020).
1038 58. Sluka, T. & Tagantsev, A. Electronic elements based on quasitwo-dimensional electron/hole
1039 gas at charged domain walls in ferroelectrics. (2014).
1040 59. Sharma, P. *et al.* Nonvolatile ferroelectric domain wall memory. *Sci. Adv.* **3**, e1700512 (2017).
1041 60. Sharma, P. *et al.* Conformational Domain Wall Switch. *Adv. Funct. Mater.* **29**, 1807523
1042 (2019).
1043 61. McConville, J. P. V. *et al.* Ferroelectric Domain Wall Memristor. *Adv. Funct. Mater.* **30**,
1044 2000109 (2020).
1045 62. Marković, D., Mizrahi, A., Querlioz, D. & Grollier, J. Physics for neuromorphic computing.
1046 *Nat. Rev. Phys.* **2**, 499–510 (2020).
1047 63. Boyn, S. *et al.* Learning through ferroelectric domain dynamics in solid-state synapses. *Nat.*
1048 *Commun.* **8**, 14736 (2017).
1049 64. Oh, S., Hwang, H. & Yoo, I. K. Ferroelectric materials for neuromorphic computing. *APL*
1050 *Mater.* **7**, 091109 (2019).

1051 65. Godau, C., Kämpfe, T., Thiessen, A., Eng, L. M. & Haußmann, A. Enhancing the Domain Wall
1052 Conductivity in Lithium Niobate Single Crystals. *ACS Nano* **11**, 4816–4824 (2017).
1053 66. Lu, H. *et al.* Electrical Tunability of Domain Wall Conductivity in $LiNbO_3$ Thin Films. *Adv.*
1054 *Mater.* **31**, 1902890 (2019).
1055 67. Chai, X. *et al.* Nonvolatile ferroelectric field-effect transistors. *Nat. Commun.* **11**, 2811
1056 (2020).
1057 68. Li, L. *et al.* Giant Resistive Switching via Control of Ferroelectric Charged Domain Walls. *Adv.*
1058 *Mater.* **28**, 6574–6580 (2016).
1059 69. Jiang, J. *et al.* Temporary formation of highly conducting domain walls for non-destructive
1060 read-out of ferroelectric domain-wall resistance switching memories. *Nat. Mater.* **17**, 49–56
1061 (2018).
1062 70. Jiang, A. Q. *et al.* Ferroelectric domain wall memory with embedded selector realized in
1063 $LiNbO_3$ single crystals integrated on Si wafers. *Nat. Mater.* 1–7 (2020) doi:10.1038/s41563-020-
1064 0702-z.
1065 71. Schröder, M. *et al.* Nanoscale and macroscopic electrical ac transport along conductive
1066 domain walls in lithium niobate single crystals. *Mater. Res. Express* **1**, 035012 (2014).
1067 72. Wu, X. *et al.* Low-energy structural dynamics of ferroelectric domain walls in hexagonal rare-
1068 earth manganites. *Sci. Adv.* **3**, e1602371 (2017).
1069 73. Wu, X. *et al.* Microwave conductivity of ferroelectric domains and domain walls in a
1070 hexagonal rare-earth ferrite. *Phys. Rev. B* **98**, 081409 (2018).
1071 74. Tselev, A. *et al.* Microwave a.c. conductivity of domain walls in ferroelectric thin films. *Nat.*
1072 *Commun.* **7**, 11630 (2016).
1073 75. Huang, Y.-L. *et al.* Unexpected Giant Microwave Conductivity in a Nominally Silent $BiFeO_3$
1074 Domain Wall. *Adv. Mater.* **32**, 1905132 (2020).
1075 76. Johnson, J. B. Thermal Agitation of Electricity in Conductors. *Phys. Rev.* **32**, 97–109 (1928).

1076 77. Nyquist, H. Thermal Agitation of Electric Charge in Conductors. *Phys. Rev.* **32**, 110–113
1077 (1928).
1078 78. Solid State Electronic Devices - Paperback - K. Bhattacharya, Rajnish Sharma - Oxford
1079 University Press.
1080 79. Turner, P. W. *et al.* Large Carrier Mobilities in $ErMnO_3$ Conducting Domain Walls Revealed by
1081 Quantitative Hall-Effect Measurements. *Nano Lett.* **18**, 6381–6386 (2018).
1082 80. Fortunato, E. *et al.* High field-effect mobility zinc oxide thin film transistors produced at
1083 room temperature. *J. Non-Cryst. Solids* **338–340**, 806–809 (2004).
1084 81. Kim, H. J. *et al.* High Mobility in a Stable Transparent Perovskite Oxide. *Appl. Phys. Express* **5**,
1085 061102 (2012).
1086 82. Huang, G., Duan, L., Dong, G., Zhang, D. & Qiu, Y. High-Mobility Solution-Processed Tin Oxide
1087 Thin-Film Transistors with High-κ Alumina Dielectric Working in Enhancement Mode. *ACS Appl.*
1088 *Mater. Interfaces* **6**, 20786–20794 (2014).
1089 83. Shih, C. W. & Chin, A. New Material Transistor with Record-High Field-Effect Mobility among
1090 Wide-Band-Gap Semiconductors. *ACS Appl. Mater. Interfaces* **8**, 19187–19191 (2016).
1091 84. Lee, J. H. *et al.* Spintronic Functionality of $BiFeO_3$ Domain Walls. *Adv. Mater.* **26**, 7078–7082
1092 (2014).
1093 85. He, Q. *et al.* Magnetotransport at Domain Walls in $BiFeO_3$. *Phys. Rev. Lett.* **108**, 067203
1094 (2012).
1095 86. Domingo, N., Farokhipoor, S., Santiso, J., Noheda, B. & Catalan, G. Domain wall
1096 magnetoresistance in $BiFeO_3$ thin films measured by scanning probe microscopy. *J. Phys. Condens.*
1097 *Matter* **29**, 334003 (2017).
1098 87. Stefani, C. *et al.* Mechanical Softness of Ferroelectric 180° Domain Walls. *Phys. Rev. X* **10**,
1099 041001 (2020).
1100 88. Ihlefeld, J. F. *et al.* Room-Temperature Voltage Tunable Phonon Thermal Conductivity via
1101 Reconfigurable Interfaces in Ferroelectric Thin Films. *Nano Lett.* **15**, 1791–1795 (2015).

1102 89. Seijas-Bellido, J. A. *et al.* A phononic switch based on ferroelectric domain walls. *Phys. Rev. B*
1103 **96**, 140101 (2017).
1104 90. Langenberg, E. *et al.* Ferroelectric Domain Walls in PbTiO3 Are Effective Regulators of Heat
1105 Flow at Room Temperature. *Nano Lett.* **19**, 7901–7907 (2019).
1106 91. Royo, M., Escorihuela-Sayalero, C., Íñiguez, J. & Rurali, R. Ferroelectric domain wall phonon
1107 polarizer. *Phys. Rev. Mater.* **1**, 051402 (2017).
1108 92. Yang, S. Y. *et al.* Above-bandgap voltages from ferroelectric photovoltaic devices. *Nat.*
1109 *Nanotechnol.* **5**, 143–147 (2010).
1110 93. Seidel, J. *et al.* Efficient Photovoltaic Current Generation at Ferroelectric Domain Walls. *Phys.*
1111 *Rev. Lett.* **107**, 126805 (2011).
1112 94. Seidel, J., Yang, S.-Y., Alarcón-Lladó, E., III, J. W. A. & Ramesh, R. Nanoscale Probing of High
1113 Photovoltages at 109° Domain Walls. *Ferroelectrics* **433**, 123–126 (2012).
1114 95. Bhatnagar, A., Roy Chaudhuri, A., Heon Kim, Y., Hesse, D. & Alexe, M. Role of domain walls in
1115 the abnormal photovoltaic effect in BiFeO 3. *Nat. Commun.* **4**, 2835 (2013).
1116 96. Yang, M.-M., Bhatnagar, A., Luo, Z.-D. & Alexe, M. Enhancement of Local Photovoltaic
1117 Current at Ferroelectric Domain Walls in BiFeO 3. *Sci. Rep.* **7**, 43070 (2017).
1118 97. Martin, L. W. & Rappe, A. M. Thin-film ferroelectric materials and their applications. *Nat.*
1119 *Rev. Mater.* **2**, 1–14 (2016).
1120 98. De Luca, G. *et al.* Nanoscale design of polarization in ultrathin ferroelectric heterostructures.
1121 *Nat. Commun.* **8**, 1419 (2017).
1122 99. Campanini, M., Erni, R. & Rossell, M. D. Probing local order in multiferroics by transmission
1123 electron microscopy. *Phys. Sci. Rev.* **5**, (2019).
1124 100. Rojac, T. *et al.* Domain-wall conduction in ferroelectric $BiFeO_3$ controlled by accumulation of
1125 charged defects. *Nat. Mater.* **16**, 322–327 (2017).
1126 101. Mundy, J. A. *et al.* Functional electronic inversion layers at ferroelectric domain walls. *Nat.*
1127 *Mater.* **16**, 622–627 (2017).

1128 102. Lee, W. T. & Salje, E. K. H. Chemical turnstile. *Appl. Phys. Lett.* **87**, 143110 (2005).

1129 103. Wu, X. & Vanderbilt, D. Theory of hypothetical ferroelectric superlattices incorporating head-
1130 to-head and tail-to-tail 180° domain walls. *Phys. Rev. B* **73**, 020103 (2006).

1131 104. Jia, C.-L. *et al.* Atomic-scale study of electric dipoles near charged and uncharged domain
1132 walls in ferroelectric films. *Nat. Mater.* **7**, 57–61 (2008).

1133 105. Cohen, R. E. Origin of ferroelectricity in perovskite oxides. *Nature* **358**, 136–138 (1992).

1134 106. King-Smith, R. D. & Vanderbilt, D. Theory of polarization of crystalline solids. *Phys. Rev. B* **47**,
1135 1651–1654 (1993).

1136 107. Van Aken, B. B., Palstra, T. T. M., Filippetti, A. & Spaldin, N. A. The origin of ferroelectricity in
1137 magnetoelectric $YMnO_3$. *Nat. Mater.* **3**, 164–170 (2004).

1138 108. Neaton, J. B., Ederer, C., Waghmare, U. V., Spaldin, N. A. & Rabe, K. M. First-principles study
1139 of spontaneous polarization in multiferroic $BiFeO_3$. *Phys. Rev. B* **71**, 014113 (2005).

1140 109. He, L. & Vanderbilt, D. First-principles study of oxygen-vacancy pinning of domain walls in
1141 $PbTiO_3$. *Phys. Rev. B* **68**, 134103 (2003).

1142 110. Pöykkö, S. & Chadi, D. J. Ab initio study of 180° domain wall energy and structure in $PbTiO_3$.
1143 *Appl. Phys. Lett.* **75**, 2830–2832 (1999).

1144 111. Wojdeł, J. C. & Íñiguez, J. Ferroelectric Transitions at Ferroelectric Domain Walls Found from
1145 First Principles. *Phys. Rev. Lett.* **112**, 247603 (2014).

1146 112. Wang, Y. J., Chen, D., Tang, Y. L., Zhu, Y. L. & Ma, X. L. Origin of the Bloch-type polarization
1147 components at the 180° domain walls in ferroelectric $PbTiO_3$. *J. Appl. Phys.* **116**, 224105 (2014).

1148 113. Liu, S., Grinberg, I. & Rappe, A. M. Intrinsic ferroelectric switching from first principles.
1149 *Nature* **534**, 360–363 (2016).

1150 114. Marton, P., Stepkova, V. & Hlinka, J. Divergence of dielectric permittivity near phase
1151 transition within ferroelectric domain boundaries. *Phase Transit.* **86**, 103–108 (2013).

1152 115. Li, M., Gu, Y., Wang, Y., Chen, L.-Q. & Duan, W. First-principles study of 180° domain walls in
1153 $BaTiO_3$: Mixed Bloch-Néel-Ising character. *Phys. Rev. B* **90**, 054106 (2014).

1154 116. Lubk, A., Gemming, S. & Spaldin, N. A. First-principles study of ferroelectric domain walls in
1155 multiferroic bismuth ferrite. *Phys. Rev. B* **80**, 104110 (2009).
1156 117. Kumagai, Y. & Spaldin, N. A. Structural domain walls in polar hexagonal manganites. *Nat.*
1157 *Commun.* **4**, 1540 (2013).
1158 118. Diéguez, O., Aguado-Puente, P., Junquera, J. & Íñiguez, J. Domain walls in a perovskite oxide
1159 with two primary structural order parameters: First-principles study of $BiFeO_3$. *Phys. Rev. B* **87**,
1160 024102 (2013).
1161 119. Småbråten, D. R. *et al.* Charged domain walls in improper ferroelectric hexagonal
1162 manganites and gallates. *Phys. Rev. Mater.* **2**, 114405 (2018).
1163 120. Íñiguez, J. First-Principles Studies of Structural Domain Walls. in *Domain Walls - From*
1164 *Fundamental Properties to Nanotechnology Concepts* 36–75 (Oxford University Press, 2020).
1165 121. Freysoldt, C. *et al.* First-principles calculations for point defects in solids. *Rev. Mod. Phys.* **86**,
1166 253–305 (2014).
1167 122. Robert, G., Damjanovic, D., Setter, N. & Turik, A. V. Preisach modeling of piezoelectric
1168 nonlinearity in ferroelectric ceramics. *J. Appl. Phys.* **89**, 5067–5074 (2001).
1169 123. Aggarwal, S. & Ramesh, R. Point Defect Chemistry of Metal Oxide Heterostructures. *Annu.*
1170 *Rev. Mater. Sci.* **28**, 463–499 (1998).
1171 124. Scott, J. F. & Dawber, M. Oxygen-vacancy ordering as a fatigue mechanism in perovskite
1172 ferroelectrics. *Appl. Phys. Lett.* **76**, 3801–3803 (2000).
1173 125. Rojac, T., Kosec, M., Budic, B., Setter, N. & Damjanovic, D. Strong ferroelectric domain-wall
1174 pinning in $BiFeO_3$ ceramics. *J. Appl. Phys.* **108**, 074107 (2010).
1175 126. Pöykkö, S. & Chadi, D. J. Ab initio study of dipolar defects and 180° domain walls in $PbTiO_3$. *J.*
1176 *Phys. Chem. Solids* **61**, 291–294 (2000).
1177 127. Paillard, C., Geneste, G., Bellaiche, L. & Dkhil, B. Vacancies and holes in bulk and at 180°
1178 domain walls in lead titanate. *J. Phys. Condens. Matter* **29**, 485707 (2017).

1179 128. Tomoda, S., Shimada, T., Ueda, T., Wang, J. & Kitamura, T. Hybrid functional study on the
1180 ferroelectricity of domain walls with O-vacancies in $PbTiO_3$. *Mech. Eng. J.* **2**, 15-00037-15–00037
1181 (2015).
1182 129. Chandrasekaran, A., Damjanovic, D., Setter, N. & Marzari, N. Defect ordering and defect–
1183 domain-wall interactions in $PbTiO_3$: A first-principles study. *Phys. Rev. B* **88**, 214116 (2013).
1184 130. Chandrasekaran, A. *et al.* Asymmetric structure of 90° domain walls and interactions with
1185 defects in $PbTiO_3$. *Phys. Rev. B* **93**, 144102 (2016).
1186 131. Li, X. Y. *et al.* Domain Wall Motion in Perovskite Ferroelectrics Studied by the Nudged Elastic
1187 Band Method. *J. Phys. Chem. C* **122**, 3091–3100 (2018).
1188 132. Lee, D. & Lee, D. The Effect of Domain Wall on Defect Energetics in Ferroelectric $LiNbO_3$ from
1189 Density Functional Theory Calculations. *J. Korean Ceram. Soc.* **53**, 312–316 (2016).
1190 133. Småbråten, D. R. *et al.* Domain wall mobility and roughening in doped ferroelectric
1191 hexagonal manganites. *Phys. Rev. Res.* **2**, 033159 (2020).
1192 134. Gong, J. J. *et al.* Interactions of charged domain walls and oxygen vacancies in $BaTiO_3$: a first-
1193 principles study. *Mater. Today Phys.* **6**, 9–21 (2018).
1194 135. Skjærvø, S. H., Småbråten, D. R., Spaldin, N. A., Tybell, T. & Selbach, S. M. Oxygen vacancies
1195 in the bulk and at neutral domain walls in hexagonal $YMnO_3$. *Phys. Rev. B* **98**, 184102 (2018).
1196 136. Barrozo, P. *et al.* Defect-Enhanced Polarization Switching in the Improper Ferroelectric
1197 $LuFeO_3$. *Adv. Mater.* **32**, 2000508 (2020).
1198 137. Skjærvø, S. H. *et al.* Interstitial oxygen as a source of p-type conductivity in hexagonal
1199 manganites. *Nat. Commun.* **7**, 13745 (2016).
1200 138. Schaab, J. *et al.* Electrical half-wave rectification at ferroelectric domain walls. *Nat.*
1201 *Nanotechnol.* **13**, 1028–1034 (2018).
1202 139. Schultheiß, J. *et al.* Intrinsic and extrinsic conduction contributions at nominally neutral
1203 domain walls in hexagonal manganites. *Appl. Phys. Lett.* **116**, 262903 (2020).

1204 140. Småbråten, D. R. *et al.* Charged domain walls in improper ferroelectric hexagonal
1205 manganites and gallates. *Phys. Rev. Mater.* **2**, 114405 (2018).
1206 141. Becher, C. *et al.* Strain-induced coupling of electrical polarization and structural defects in
1207 $SrMnO_3$ films. *Nat. Nanotechnol.* **10**, 661–665 (2015).
1208 142. Schaab, J. *et al.* Contact-Free Mapping of Electronic Transport Phenomena of Polar Domains
1209 in $SrMnO_3$ Films. *Phys. Rev. Appl.* **5**, 054009 (2016).
1210 143. Bencan, A. *et al.* Domain-wall pinning and defect ordering in $BiFeO_3$ probed on the atomic
1211 and nanoscale. *Nat. Commun.* **11**, 1762 (2020).
1212 144. Farokhipoor, S. & Noheda, B. Local conductivity and the role of vacancies around twin walls
1213 of (001)−$BiFeO_3$ thin films. *J. Appl. Phys.* **112**, 052003 (2012).
1214 145. Noguchi, Y., Matsuo, H., Kitanaka, Y. & Miyayama, M. Ferroelectrics with a controlled
1215 oxygen-vacancy distribution by design. *Sci. Rep.* **9**, 4225 (2019).
1216 146. Sturman, B. & Podivilov, E. Ion and mixed electron-ion screening of charged domain walls in
1217 ferroelectrics. *EPL Europhys. Lett.* **122**, 67005 (2018).
1218 147. Stolichnov, I. *et al.* Persistent conductive footprints of 109° domain walls in bismuth ferrite
1219 films. *Appl. Phys. Lett.* **104**, 132902 (2014).
1220 148. Han, M.-G. *et al.* Interface-induced nonswitchable domains in ferroelectric thin films. *Nat.*
1221 *Commun.* **5**, 4693 (2014).
1222 149. Sanchez-Santolino, G. *et al.* Resonant electron tunnelling assisted by charged domain walls in
1223 multiferroic tunnel junctions. *Nat. Nanotechnol.* **12**, 655–662 (2017).
1224 150. Farokhipoor, S. *et al.* Artificial chemical and magnetic structure at the domain walls of an
1225 epitaxial oxide. *Nature* **515**, 379–383 (2014).
1226 151. Paruch, P. & Guyonnet, J. Nanoscale studies of ferroelectric domain walls as pinned elastic
1227 interfaces. *Comptes Rendus Phys.* **14**, 667–684 (2013).
1228 152. Paruch, P., Giamarchi, T. & Triscone, J.-M. Domain Wall Roughness in Epitaxial Ferroelectric
1229 $PbZr_{0.2}Ti_{0.8}O_3$ Thin Films. *Phys. Rev. Lett.* **94**, 197601 (2005).

1230 153. Fiebig, M., Lottermoser, T., Meier, D. & Trassin, M. The evolution of multiferroics. *Nat. Rev.*
1231 *Mater.* **1**, 1–14 (2016).
1232 154. Crassous, A., Sluka, T., Tagantsev, A. K. & Setter, N. Polarization charge as a reconfigurable
1233 quasi-dopant in ferroelectric thin films. *Nat. Nanotechnol.* **10**, 614–618 (2015).
1234 155. Ruff, A. *et al.* Frequency dependent polarisation switching in h-$ErMnO_3$. *Appl. Phys. Lett.* **112**,
1235 182908 (2018).
1236 156. Jungk, T., Hoffmann, Á., Fiebig, M. & Soergel, E. Electrostatic topology of ferroelectric
1237 domains in $YMnO_3$. *Appl. Phys. Lett.* **97**, 012904 (2010).
1238 157. Han, M.-G. *et al.* Ferroelectric Switching Dynamics of Topological Vortex Domains in a
1239 Hexagonal Manganite. *Adv. Mater.* **25**, 2415–2421 (2013).
1240 158. Wang, X. *et al.* Unfolding of Vortices into Topological Stripes in a Multiferroic Material. *Phys.*
1241 *Rev. Lett.* **112**, 247601 (2014).
1242 159. Xue, F., Wang, X., Shi, Y., Cheong, S.-W. & Chen, L.-Q. Strain-induced incommensurate
1243 phases in hexagonal manganites. *Phys. Rev. B* **96**, 104109 (2017).
1244 160. Campbell, M. P. *et al.* Hall effect in charged conducting ferroelectric domain walls. *Nat.*
1245 *Commun.* **7**, 13764 (2016).
1246 161. Coeuré, Ph., Guinet, P., Peuzin, J. C., Buisson, G. & Bertaut, E. F. *Ferroelectric properties of*
1247 *hexagonal orthomanganites of yttrium and rare earths*. vol. 1 (Proceedings of the International
1248 Meeting on Ferroelectricity, 1966).
1249 162. Fennie, C. J. & Rabe, K. M. Ferroelectric transition in $YMnO_3$ from first principles. *Phys. Rev. B*
1250 **72**, 100103 (2005).
1251 163. Lilienblum, M. *et al.* Ferroelectricity in the multiferroic hexagonal manganites. *Nat. Phys.* **11**,
1252 1070–1073 (2015).
1253 164. Meier, D. *et al.* Translation domains in multiferroics. *Phase Transit.* **86**, 33–52 (2013).
1254 165. Holtz, M. E. *et al.* Topological Defects in Hexagonal Manganites: Inner Structure and
1255 Emergent Electrostatics. *Nano Lett.* **17**, 5883–5890 (2017).

1256 166. Schoenherr, P. *et al.* Observation of Uncompensated Bound Charges at Improper
1257 Ferroelectric Domain Walls. *Nano Lett.* **19**, 1659–1664 (2019).
1258 167. Schaab, J. *et al.* Electrostatic potential mapping at ferroelectric domain walls by low-
1259 temperature photoemission electron microscopy. *Appl. Phys. Lett.* **115**, 122903 (2019).
1260 168. Kuerten, L. *et al.* Local control of improper ferroelectric domains in $YMnO_3$. *Phys. Rev. B* **102**,
1261 094108 (2020).
1262 169. Griffin, S. M. *et al.* Scaling Behavior and Beyond Equilibrium in the Hexagonal Manganites.
1263 *Phys. Rev. X* **2**, 041022 (2012).
1264 170. Meier, Q. N. *et al.* Global Formation of Topological Defects in the Multiferroic Hexagonal
1265 Manganites. *Phys. Rev. X* **7**, 041014 (2017).
1266 171. Chae, S. C. *et al.* Direct Observation of the Proliferation of Ferroelectric Loop Domains and
1267 Vortex-Antivortex Pairs. *Phys. Rev. Lett.* **108**, 167603 (2012).
1268 172. Salje, E. K. H. Robust templates for domain boundary engineering in $ErMnO_3$. *New J. Phys.*
1269 **18**, 051001 (2016).
1270 173. Hassanpour, E. *et al.* Robustness of magnetic and electric domains against charge carrier
1271 doping in multiferroic hexagonal $ErMnO_3$. *New J. Phys.* **18**, 043015 (2016).
1272 174. Du, Y. *et al.* Manipulation of domain wall mobility by oxygen vacancy ordering in multiferroic
1273 $YMnO_3$. *Phys. Chem. Chem. Phys.* **15**, 20010 (2013).
1274 175. Li, J. *et al.* Scanning secondary-electron microscopy on ferroelectric domains and domain
1275 walls in $YMnO_3$. *Appl. Phys. Lett.* **100**, 152903 (2012).
1276 176. Remsen, S. & Dabrowski, B. Synthesis and Oxygen Storage Capacities of Hexagonal Dy_{1-}
1277 $_{x}Y_xMnO_{3+\delta}$. *Chem. Mater.* **23**, 3818–3827 (2011).
1278 177. Świerczek, K. *et al.* Oxygen storage properties of hexagonal $HoMnO_{3+\delta}$. *Phys. Chem. Chem.*
1279 *Phys.* **19**, 19243–19251 (2017).
1280 178. Evans, D. M. *et al.* Conductivity control via minimally invasive anti-Frenkel defects in a
1281 functional oxide. *Nat. Mater.* (2020) doi:10.1038/s41563-020-0765-x.

1282 179. Mosberg, A. B. *et al.* FIB lift-out of conducting ferroelectric domain walls in hexagonal
1283 manganites. *Appl. Phys. Lett.* **115**, 122901 (2019).
1284 180. Pang, H. *et al.* Preparation of epitaxial hexagonal $YMnO_3$ thin films and observation of
1285 ferroelectric vortex domains. *Npj Quantum Mater.* **1**, 16015 (2016).
1286 181. Nordlander, J. *et al.* The ultrathin limit of improper ferroelectricity. *Nat. Commun.* **10**, 5591
1287 (2019).
1288 182. Småbråten, D. R., Nakata, A., Meier, D., Miyazaki, T. & Selbach, S. M. First-principles study of
1289 topologically protected vortices and ferroelectric domain walls in hexagonal YGaO 3. *Phys. Rev. B*
1290 **102**, 144103 (2020).
1291 183. Wang, W. *et al.* Room-Temperature Multiferroic Hexagonal $LuFeO_3$ Films. *Phys. Rev. Lett.*
1292 **110**, 237601 (2013).
1293 184. Das, H., Wysocki, A. L., Geng, Y., Wu, W. & Fennie, C. J. Bulk magnetoelectricity in the
1294 hexagonal manganites and ferrites. *Nat. Commun.* **5**, 2998 (2014).
1295 185. McNulty, J. A. *et al.* An Electronically Driven Improper Ferroelectric: Tungsten Bronzes as
1296 Microstructural Analogs for the Hexagonal Manganites. *Adv. Mater.* **31**, 1903620 (2019).
1297 186. Mundy, J. A. *et al.* Atomically engineered ferroic layers yield a room-temperature
1298 magnetoelectric multiferroic. *Nature* **537**, 523–527 (2016).
1299 187. Holtz, M. E. *et al.* Dimensionality-induced change in topological order in multiferroic oxide
1300 superlattices. *ArXiv200703872 Cond-Mat* (2020).
1301 188. Benedek, N. A. & Fennie, C. J. Hybrid Improper Ferroelectricity: A Mechanism for
1302 Controllable Polarization-Magnetization Coupling. *Phys. Rev. Lett.* **106**, 107204 (2011).
1303 189. Mulder, A. T., Benedek, N. A., Rondinelli, J. M. & Fennie, C. J. Turning ABO_3 Antiferroelectrics
1304 into Ferroelectrics: Design Rules for Practical Rotation-Driven Ferroelectricity in Double
1305 Perovskites and $A_3B_2O_7$ Ruddlesden-Popper Compounds. *Adv. Funct. Mater.* **23**, 4810–4820
1306 (2013).

1307 190. Moritomo, Y., Asamitsu, A., Kuwahara, H. & Tokura, Y. Giant magnetoresistance of
1308 manganese oxides with a layered perovskite structure. *Nature* **380**, 141–144 (1996).
1309 191. Tarascon, J. M., Greene, L. H., Mckinnon, W. R., Hull, G. W. & Geballe, T. H.
1310 Superconductivity at 40 K in the Oxygen-Defect Perovskites $La_{2-x}Sr_xCuO_{4-y}$. *Science* **235**, 1373–1376
1311 (1987).
1312 192. Meyer, G. M., Nelmes, R. J., Thornley, F. R. & Stirling, W. G. An inelastic neutron-scattering
1313 study of the improper ferroelectric transition in copper chlorine boracite. *J. Phys. C Solid State*
1314 *Phys.* **15**, 2851–2866 (1982).
1315 193. Cochard, C. *et al.* Anomalous Domain Wall Motion in Copper-Chlorine Boracite—A New
1316 Opportunity in Negative Capacitance? (2019).
1317 194. Sergienko, I. A. & Dagotto, E. Role of the Dzyaloshinskii-Moriya interaction in multiferroic
1318 perovskites. *Phys. Rev. B* **73**, 094434 (2006).
1319 195. Katsura, H., Nagaosa, N. & Balatsky, A. V. Spin Current and Magnetoelectric Effect in
1320 Noncollinear Magnets. *Phys. Rev. Lett.* **95**, 057205 (2005).
1321 196. Mostovoy, M. Ferroelectricity in Spiral Magnets. *Phys. Rev. Lett.* **96**, 067601 (2006).
1322 197. Newnham, R. E., Kramer, J. J., Schulze, W. A. & Cross, L. E. Magnetoferroelectricity in Cr
1323 $_2BeO_4$. *J. Appl. Phys.* **49**, 6088–6091 (1978).
1324 198. Kimura, T. *et al.* Magnetic control of ferroelectric polarization. *Nature* **426**, 55–58 (2003).
1325 199. Hur, N. *et al.* Electric polarization reversal and memory in a multiferroic material induced by
1326 magnetic fields. *Nature* **429**, 392–395 (2004).
1327 200. Lawes, G. *et al.* Magnetically Driven Ferroelectric Order in $Ni_3V_2O_8$. *Phys. Rev. Lett.* **95**,
1328 087205 (2005).
1329 201. Arkenbout, A. H., Palstra, T. T. M., Siegrist, T. & Kimura, T. Ferroelectricity in the cycloidal
1330 spiral magnetic phase of $MnWO_4$. *Phys. Rev. B* **74**, 184431 (2006).
1331 202. Kimura, T., Sekio, Y., Nakamura, H., Siegrist, T. & Ramirez, A. P. Cupric oxide as an induced-
1332 multiferroic with high-T_C. *Nat. Mater.* **7**, 291–294 (2008).

1333 203. Tokunaga, Y., Iguchi, S., Arima, T. & Tokura, Y. Magnetic-Field-Induced Ferroelectric State in
1334 $DyFeO_3$. *Phys. Rev. Lett.* **101**, 097205 (2008).
1335 204. Tokura, Y., Seki, S. & Nagaosa, N. Multiferroics of spin origin. *Rep. Prog. Phys.* **77**, 076501
1336 (2014).
1337 205. Kimura, T. Spiral Magnets as Magnetoelectrics. *Annu. Rev. Mater. Res.* **37**, 387–413 (2007).
1338 206. Meier, D. *et al.* Observation and Coupling of Domains in a Spin-Spiral Multiferroic. *Phys. Rev.*
1339 *Lett.* **102**, 107202 (2009).
1340 207. Meier, D. *et al.* Topology and manipulation of multiferroic hybrid domains in $MnWO_4$. *Phys.*
1341 *Rev. B* **80**, 224420 (2009).
1342 208. Leo, N. *et al.* Polarization control at spin-driven ferroelectric domain walls. *Nat. Commun.* **6**,
1343 6661 (2015).
1344 209. Matsubara, M. *et al.* Magnetoelectric domain control in multiferroic $TbMnO_3$. *Science* **348**,
1345 1112–1115 (2015).
1346 210. Wu, W. *et al.* Polarization-Modulated Rectification at Ferroelectric Surfaces. *Phys. Rev. Lett.*
1347 **104**, 217601 (2010).
1348 211. Manz, S. *et al.* Reversible optical switching of antiferromagnetism in $TbMnO_3$. *Nat. Photonics*
1349 **10**, 653–656 (2016).
1350 212. Rocquefelte, X., Schwarz, K., Blaha, P., Kumar, S. & van den Brink, J. Room-temperature spin-
1351 spiral multiferroicity in high-pressure cupric oxide. *Nat. Commun.* **4**, 2511 (2013).
1352 213. Johnson, R. D. *et al.* Giant Improper Ferroelectricity in the Ferroaxial Magnet $CaMn_7O_{12}$.
1353 *Phys. Rev. Lett.* **108**, 067201 (2012).
1354 214. Kitagawa, Y. *et al.* Low-field magnetoelectric effect at room temperature. *Nat. Mater.* **9**,
1355 797–802 (2010).
1356 215. Aoyama, T. *et al.* Giant spin-driven ferroelectric polarization in $TbMnO_3$ under high pressure.
1357 *Nat. Commun.* **5**, 4927 (2014).

1358 216. Cherifi-Hertel, S. *et al.* Non-Ising and chiral ferroelectric domain walls revealed by nonlinear
1359 optical microscopy. *Nat. Commun.* **8**, 15768 (2017).
1360 217. Sheng, Y., Best, A., Arie, A. & Koynov, K. Three-dimensional ferroelectric domain visualization
1361 by Cherenkov-type second harmonic generation. 7 (2010).
1362 218. Kämpfe, T. *et al.* Optical three-dimensional profiling of charged domain walls in ferroelectrics
1363 by Cherenkov second-harmonic generation. *Phys. Rev. B* **89**, 035314 (2014).
1364 219. Simons, H. *et al.* Dark-field X-ray microscopy for multiscale structural characterization. *Nat.*
1365 *Commun.* **6**, 6098 (2015).
1366 220. Nan, N. & Wang, J. FIB-SEM Three-Dimensional Tomography for Characterization of Carbon-
1367 Based Materials. *Advances in Materials Science and Engineering*
1368 https://www.hindawi.com/journals/amse/2019/8680715/ (2019).
1369 221. Xu, X. *et al.* Variability and origins of grain boundary electric potential detected by electron
1370 holography and atom-probe tomography. *Nat. Mater.* **19**, 887–893 (2020).
1371 222. Nakata, A. *et al.* Large scale and linear scaling DFT with the CONQUEST code. *J. Chem. Phys.*
1372 **152**, 164112 (2020).
1373 223. Kalinin, S. V. & Spaldin, N. A. Functional Ion Defects in Transition Metal Oxides. *Science* **341**,
1374 858–859 (2013).
1375 224. Catalan, G. *et al.* Flexoelectric rotation of polarization in ferroelectric thin films. *Nat. Mater.*
1376 **10**, 963–967 (2011).
1377 225. Gu, Y. *et al.* Flexoelectricity and ferroelectric domain wall structures: Phase-field modeling
1378 and DFT calculations. *Phys. Rev. B* 11 (2014).
1379 226. Schiaffino, A. & Stengel, M. Macroscopic Polarization from Antiferrodistortive Cycloids in
1380 Ferroelastic $SrTiO_3$. *Phys. Rev. Lett.* **119**, 137601 (2017).
1381 227. Xu, T., Shimada, T., Araki, Y., Wang, J. & Kitamura, T. Multiferroic Domain Walls in
1382 Ferroelectric $PbTiO_3$ with Oxygen Deficiency. *Nano Lett.* **16**, 454–458 (2016).

1383 228. Trassin, M. Low energy consumption spintronics using multiferroic heterostructures. *J. Phys.*
1384 *Condens. Matter* **28**, 033001 (2015).
1385 229. Becher, C. *et al.* Functional ferroic heterostructures with tunable integral symmetry. *Nat.*
1386 *Commun.* **5**, 4295 (2014).
1387 230. Bakaul, S. R. *et al.* Ferroelectric Domain Wall Motion in Freestanding Single-Crystal Complex
1388 Oxide Thin Film. *Adv. Mater.* **32**, 1907036 (2020).
1389 231. Aizu, K. Possible Species of Ferromagnetic, Ferroelectric, and Ferroelastic Crystals. *Phys. Rev.*
1390 *B* **2**, 754–772 (1970).
1391 232. Wadhawan, V. *Introduction to Ferroic Materials*. (CRC Press, 2000).
1392 233. Tolédano, J. C. & Tolédano, P. *The Landau Theory of Phase Transitions: Application to*
1393 *Structural, Incommensurate, Magnetic and Liquid Crystal Systems*. vol. 3 (WORLD SCIENTIFIC,
1394 1987).
1395 234. Keve, E. T., Abrahams, S. C. & Bernstein, J. L. Ferroelectric Ferroelastic Paramagnetic Beta-
1396 $Gd_2(MoO_4)_3$ Crystal Structure of the Transition-Metal Molybdates and Tungstates. VI. *J. Chem.*
1397 *Phys.* **54**, 3185–3194 (1971).
1398 235. Kalinin, S. V., Borisevich, A. & Fong, D. Beyond Condensed Matter Physics on the Nanoscale:
1399 The Role of Ionic and Electrochemical Phenomena in the Physical Functionalities of Oxide
1400 Materials. *ACS Nano* **6**, 10423–10437 (2012).
1401 236. Smyth, D. M. *The Defect Chemistry of Metal Oxides*. (Oxford University Press, 2000).
1402 237. Maier, J. *Physical Chemistry of Ionic Materials: Ions and Electrons in Solids*. (Wiley, 2004).
1403 238. Grande, T., Tolchard, J. R. & Selbach, S. M. Anisotropic Thermal and Chemical Expansion in
1404 Sr-Substituted $LaMnO_{3+\delta}$: Implications for Chemical Strain Relaxation. *Chem. Mater.* **24**, 338–345
1405 (2012).
1406
1407